Energy Research and Development Division

FINAL PROJECT REPORT

Accelerating the Development of Liquid Fuels Directly from Sunlight

California Energy Commission

Edmund G. Brown Jr., Governor

February 2018 | CEC-500-2018-003

PREPARED BY:

Primary Author(s):

Xenia Amashukeli
Joel Ager
Wesley Kramer
Alex Bell
Charles McCrory
Frances Houle
Gael Ung
Daniel Miller
Harry Gray
John Gregoire
James Blakemore

Joint Center for Artificial Photosynthesis
California Institute of Technology
1200 E. California Blvd.
Pasadena, CA 91125
www.solarfuelshub.org

Agreement Number: 500-11-023

PREPARED FOR:
California Energy Commission

Reynaldo Gonzalez
Contract Manager

Aleecia Gutierrez
Office Manager
ENERGY GENERATION RESEARCH OFFICE

Laurie ten Hope
Deputy Director
ENERGY RESEARCH AND DEVELOPMENT DIVISION

Drew Bohan
Executive Director

PREFACE

The California Energy Commission entered into an agreement through the Alternative Renewable Fuel Vehicle Technology (ARFVT) Program with California Institute of Technology to accelerate developing liquid fuels directly from sunlight through molecular catalysts and membranes. Assembly Bill 118 (Núñez, Chapter 750, Statutes of 2007), created the ARFVT Program. The statute, amended by AB 109 (Núñez) Chapter 313, Statutes of 2008), authorizes the California Energy Commission to develop and deploy alternative and renewable fuels and advanced transportation technologies to help attain the state's climate change policies. The Energy Commission provides financial support for projects that:

- Develop and improve alternative and renewable low-carbon fuels.
- Enhance alternative and renewable fuels for existing and developing engine technologies.
- Produce alternative and renewable low-carbon fuels in California.
- Decrease, on a full-fuel-cycle basis, the overall impact and carbon footprint of alternative and renewable fuels and increase sustainability.
- Expand fuel infrastructure, fueling stations, and equipment.
- Improve light-, medium-, and heavy-duty vehicle technologies.
- Retrofit medium- and heavy-duty on-road and non-road vehicle fleets.
- Expand infrastructure connected with existing fleets, public transit, and transportation corridors.
- Establish workforce training programs, conduct public education and promotion, and create technology centers.

To be eligible for funding this project was consistent with the Energy Commission's ARFVT Investment Plan, updated annually. In response to the technological needs identified in the ARFVTP Investment Plan (2010/2011), Caltech jointly developed an agreement with the Energy Commission , which was proposed for funding and approved at the May 5, 2012, Business Meeting, and the agreement was executed as 500-11-023 on November 27, 2013.

ABSTRACT

Led by California Institute of Technology (Caltech) in partnership with Lawrence Berkeley National Laboratory (LBNL), this research work augmented the efforts of the Joint Center for Artificial Photosynthesis (JCAP) – a U.S. Department of Energy Innovation Hub to advance developing molecular catalysts for a complete system that can produce fuel from sunlight, water and carbon dioxide (CO_2). During the term of the project, the research team studied and successfully identified selective and active catalysts encapsulated in polymeric films; developed a combined electro-polymerization system for rapid synthesis and a combinatorial fuel detection system to identify electrode materials that can produce fuels; and developed new synthetic and testing methodologies and new polymer platforms. The team has also established new techniques to control membrane synthesis and measure permeation of organic species through the membranes. These findings provide insight into strategies for synthesis and selection of materials that are necessary to further develop artificial photosynthesis systems for a viable solar-fuels technology.

Keywords: California Energy Commission, JCAP, artificial photosynthesis, carbon dioxide, solar fuels, catalysts, combinatorial synthesis and detection, membranes.

Amashukeli, Xenia; Wesley Kramer, Charles McCrory, Gael Ung, Harry Gray, James Blakemore, Joel Ager, Alex Bell, Frances Houle, Daniel Miller, John Gregoire. Joint Center for Artificial Photosynthesis, Caltech and LBNL. 2018. *Accelerating the Development of Liquid Fuels Directly from Sunlight.* California Energy Commission. Publication Number: CEC-500-2018-003.

TABLE OF CONTENTS

LIST OF FIGURES

Page

LIST OF TABLES

Page

EXECUTIVE SUMMARY

Introduction

California is one of the largest consumers of transportation fuel in the world. Developing low-carbon fuels that can meet the transportation energy demand while also reducing emissions is critical for energy and environmental security worldwide. Artificial photosynthesis can generate fuel directly from sunlight, water, and carbon dioxide, and with efficiency greater than natural plants. A typical artificial photosynthesis device – a solar-fuels generator – is a cell that consists of multiple functional components, such as light absorbers, catalysts, and membranes, and links together many different photo electrochemical processes.

In 2010, the U.S. Department of Energy (DOE) established the Joint Center for Artificial Photosynthesis, an Energy Innovation Hub led by the California Institute of Technology (Caltech) in partnership with Lawrence Berkeley National Laboratory. More than 100 scientists at the Joint Center for Artificial Photosynthesis focus on solving the challenges associated with artificial photosynthesis including developing efficient and selective catalysts and other materials, such as membranes, for complete solar-to-fuels generating systems.

Project Purpose and Process

This project complemented the efforts of Joint Center for Artificial Photosynthesis to develop new catalytic systems and membrane platforms, new product detection devices and instruments, and accelerate identifying these materials. It is integral to renewable fuel production to identify an advanced and more selective catalytic system capable of reducing CO_2 to directly form liquid fuels such as hydrocarbons and alcohols.

There are currently no known catalysts with the required characteristics suitable to use in large-scale reactors. The team focused on investigating molecular systems and the role these systems play in reducing carbon dioxide. Several approaches were used including encapsulating molecular catalysts in polymeric films (elements combined in the same proportion but with different molecular weight), immobilizing catalysts on electrode surfaces, investigating new chemical systems for CO_2 catalysis (accelerating a chemical reaction), studying the local environments' effects from reducing CO_2 with carbon-support systems, and using molecular systems as tools to modulate catalytic activities of certain transition metals, such as copper.

The team also designed an apparatus to detect and analyze liquid and gas products that form during the CO_2 reduction reactions. Certain catalysts, such as cobalt phthalocyanine, are not remarkable, however they show activity and selectivity when encapsulated into polymeric matrices. Encapsulation may also provide additional means of concentrating carbon dioxide. The results of studying zero-valent iron and cobalt complexes indicate that high energy organic molecules can serve as pre-catalysts for CO_2 reduction.

To accelerate the discovery of new catalysts, the team focused on developing high throughput combinatorial synthesis and detection for new materials. These high throughput capabilities allow for an efficient method of synthesizing and testing numerous electrodes. The team

developed two sets of instruments: a combined electro-polymerization system for rapid synthesis and an integrated fuel detection system to identify electrode materials that can produce fuels.

New solar fuels membranes are required for CO_2 reduction applications that successfully block crossover of organic products while allowing ions to pass. Creating new membrane families requires several steps: design of new polymer compositions, design of a synthetic strategy to achieve the desired molecular structure and molecular weight distribution, and design of new testing methodologies to enable separations performance to be assessed.

The team made significant progress toward creating new membrane materials and characterizing them, including identifying promising new membrane architectures, and developing a novel permeation measurement technique for mass transfer through a membrane to determine which materials are more conducive for separating products.

Results

The Joint Center for Artificial Photosynthesis made significant progress in developing an artificial synthesis conversion process. The results and accomplishments of this research are as follows:

- The team identified and developed suitable membranes for product separation through innovative transport measurement methods that dramatically improve the selectivity and activity of the CO_2-reducing catalyst.
- Zero-valent iron and cobalt complexes were further investigated as potential catalysts, and the catalyzed CO_2 reaction was observed using various experimental methods and techniques.

Additional research efforts were targeted towards developing the first high throughput-screening platform to efficiently synthesize and assess electrodes to integrate in solar fuels generator. Through automated fuel production and detection experiments, the high throughput capabilities have increased the experiment rate by a factor of 10.

- A new methodology to determine copolymerization reactivity ratios and measure permeation was developed to further characterize membrane capability.

Benefits to California

This project supports research efforts to accelerate the Joint Center for Artificial Photosynthesis work on artificial photosynthesis, and informs current and future research. Energy Commission investment in membranes research, for example, has led to a family of new membranes tailored for use in solar fuels systems, and is currently under evaluation at Joint Center for Artificial Photosynthesis. Furthermore, product measurement methodologies developed with Energy Commission funding have established a crucial foundation for the Joint Center for Artificial Photosynthesis new electrochemistry program, and continues to be used today. Artificial photosynthesis research supported with Energy Commission and DOE funding provides a pathway to recycle CO_2 emitted to the atmosphere during combustion. When this

technology is coupled with effective CO_2 capture and sequestration technologies, the development and optimization of artificial photosynthesis has the potential to play an important role in helping California meet its strict greenhouse gas emission reduction targets, reduce California's dependence on foreign energy supply, and ensure environmental sustainability. When commercialized, the artificial photosynthesis conversion process is expected to be more environmentally friendly, energy efficient and cost-effective when compared to other alternative technologies such as electrolyzers that convert CO_2 into fuels. Furthermore, advancing the science of artificial photosynthesis will expand California's renewable fuel production portfolio.

CHAPTER 1:
Task 2: Laboratory Establishment Directed to CO_2RR Research

1.1 California Institute of Technology, Laboratory Readiness

Under Task 2, California Institute of Technology (Caltech/CIT) has set up two laboratories for the California Energy Commission contract (Agreement Number 500-11-023) in support of two research activities: Tasks 3 and 4. The focus of Task 3 is to expand efforts in the development of CO_2RR Molecular Catalysts (MolCat) for liquid fuel production. The Task 3 work is performed at Caltech, Jorgensen Laboratory Building, Room 208. The research scope of Task 4 is to develop High Throughput Screening (HTS) capability. The Task 4 work is performed at Caltech, Jorgensen Laboratory Building, Room 216. The list of the equipment acquired is provided in Table 1.

1.1.1 CIT: CO_2RR Molecular Catalysts Laboratory

Task 3 is focused on the study of surface-immobilized molecular electro-catalysts for the reduction of CO_2 to liquid fuels. To accomplish Task 3 research goals, the capabilities, including electrochemical characterization of molecular catalysts and their products, have been successfully established.

A fume hood has been outfitted with a Schlenk manifold and vacuum pump that can be used to perform air-free syntheses of catalysts (Figure 1). Additionally, researchers have access to the Nitrogen glove box, which can be used for the synthesis and handling of air sensitive materials. A chemical resistant table was purchased on which to stage experiments and conduct bench-top chemistry. The required laboratory supplies included synthesis glassware and basic supplies, such as stirring hotplates. The MolCat acts as a fully independent synthetic laboratory

Characterizing compounds can be accomplished by leveraging the pre-existing instruments and facilities at JCAP and Caltech, where researchers have access to UV-Vis and FT-IR spectrometers for the analysis of molecular compounds, as well as an X-ray photoelectron spectrometer (XPS) for the analysis of surface-immobilized catalysts. On Caltech campus, researchers have access to a number of other instrument facilities that can be employed to characterize compounds, including nuclear magnetic resonance (NMR) spectrometers, mass spectrometers, and an X-ray crystallography facility.

In addition to leveraged instruments and facilities, the California Energy Commission supported developing electro-catalysis capabilities. Electrochemical analyses of the CO_2RR catalysts are conducted using two BioLogic-200 potentiostats and control computers with two electrode rotators purchased from Pine Instrument Company (Figure 2). One of the potentiostats has been mounted on a cart so that experiments in non-aqueous organic solvents can be conducted in a fume hood or in the nitrogen glove box (Figure 3). The equipment is used by researchers to investigate the electrochemical properties of catalysts under N_2 and CO_2

atmospheres, make CO_2RR kinetics measurements, and run bulk electrolysis experiments to determine and quantify the products of CO_2RR.

Table 1: CIT: List of Equipment and Instruments Procured Under Agreement

Item description (make and model)	Task #	Location	Vendor	PO#	Price per unit	Number of units	Date purchased	Date received	Total Price
Electrode Rotator	3	CIT-Jorgensen 208	Pine Research	68CEC-S198873	$5,355.00	2	4/8/14	4/16/14	$10,710.00
600 Potentiostat/Galvanostat	4	CIT-Jorgensen 216	Gamry Instruments	68CEC-S202300	$9,820.00	1	5/8/14	5/19/14	$9,820.00
Surface Attachment Potentiostat	3	CIT-Jorgensen 208	BioLogic USA	68CEC-S198658	$7,838.51	2	5/9/14	5/18/14	$15,677.01
Gaseous Fuel Detection	4	CIT-Jorgensen 216	Hiden	68CEC-S203281	$70,000.00	1	5/15/14		$70,000.00
HPR-40 MIMS Probe	4	CIT-Jorgensen 216	Hiden	68CEC-203660	$8,865.00	1	5/15/14		$8,865.00
600 Potentiostat/Galvanostat	4	CIT-Jorgensen 216	Gamry Instruments	68CEC-S210635	$9,820.00	1	7/24/14	8/14/14	$9,820.00
Polisher	4	CIT-Jorgensen 216	Labmaster	Req# 54714569	$13,584.00	1	9/29/14		$13,584.00

Figure 1: Fume Hood with Schlenk Manifold

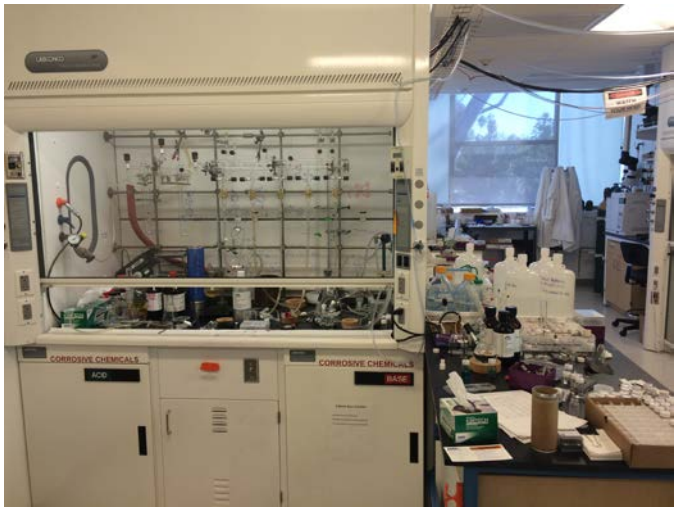

Figure 2: The Two Pine Rotators and One of the Biologic Potentiostats

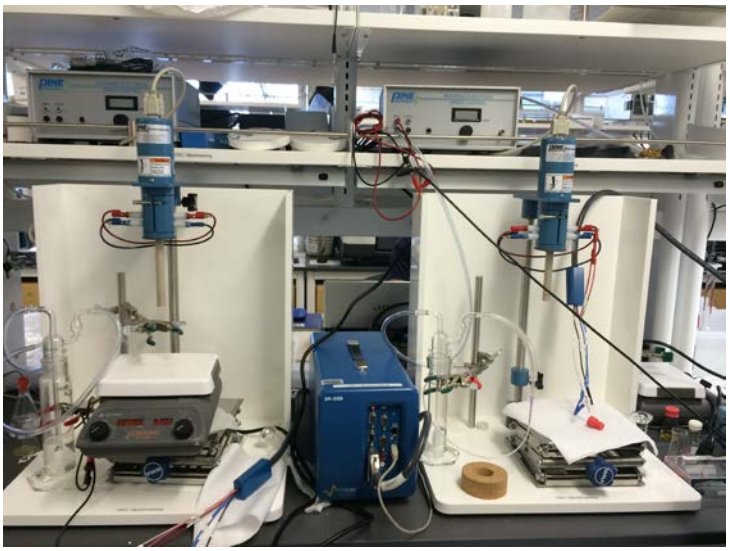

Figure 3: Cart-Mounted Biologic Potentiostat and Control PC

The research team uses three electrochemical cells to run a variety of electrochemical experiments (Figure 4). The cells were fabricated at Caltech's glass and machine shop facilities. The first cell is a one-compartment cell used in the preparation of electro polymerized catalyst films. The second cell is a two-compartment cell in which the counter electrode is separated from the reference and working electrodes by a glass frit. The cell has been used for kinetic studies of surface immobilized catalysts. An airtight, bulk electrolysis cell is used for CO_2RR product analysis in both the liquid and gas phases. In this cell design, the counter electrode is separated from the CO_2 saturated catholyte solution by a gas impermeable Nafion or Selemion membrane.

Figure 4: Electrochemical Cells Used to Study Catalytic Properties of Materials

From left to right: Electro polymerization cell, RDE cell, bulk electrolysis cell.

Different reference and working electrodes were purchased, including $Ag/AgNO_3$ non-aqueous reference electrode kits from BioAnalytical Systems, Inc., to study homogeneous molecular species and electro polymerization experiments, which are conducted in non-aqueous solvents. For experiments conducted in water, a standard reference saturated calomel electrode (SCE)

from CH-Instruments is used. To perform exploratory electrochemical experiments in aqueous and non-aqueous solutions, 3-mm diameter glassy carbon working electrodes from BioAnalytical Systems, Inc., were purchased. The majority of CO_2RR electrochemical experiments employ 5-mm diameter glassy carbon (HTW Hochtemperatur-Werkstoffe GmbH), edge-plane graphite (EPG) and basal-plane graphite (BPG) electrodes (Pine Instrument Company).

The glassy carbon discs are used for electrochemical deposition. The EPG and BPG discs are used for films prepared by drop casting or chemisorption techniques. These electrodes fit into standard U-cup fittings and can be used with the electrode rotators for rotating disk electrode (RDE) and rotating ring-disk electrode (RRDE) experiments. The team has the capacity to perform up to four RDE experiments at one time.

Procedures were developed to determine and quantify CO_2RR products in the gas and liquid phases. Gas-phase product analysis is accomplished using a Gas Chromatograph (GC) from Agilent Technologies. Using this technique, producing gaseous products such as hydrogen, ethylene, methane and carbon monoxide can be detected and quantified. Liquid products are analyzed using liquid gas chromatographs (LGC) from Agilent Technologies (Figure 5), solvent suppression NMR spectroscopy, and chemical colorimetric determination techniques. The LGC allows detection of liquid products, including alcohols, aldehydes and ketones. NMR is used as the primary method for the detection of formic acid/formate. Formaldehyde can be detected using chromotropic acid test, which is a chemical colorimetric test. UV-Vis spectroscopy is used to detect the highly colored product of the reaction of formaldehyde and chromotropic acid. In summary, all equipment and the laboratory for CO_2RR catalyst synthesis and characterization are fully operational.

Figure 5: Gas Chromatographs for Gaseous (left) and Liquid (right) Product Analysis

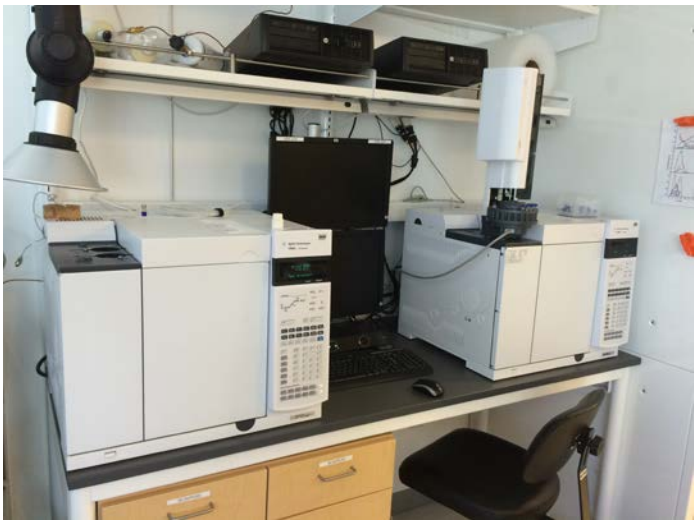

1.1.2 CIT: High-Throughput Experimentation Laboratory

The focus of high throughput experimentation (HTE) is geared toward discovery of new catalysts that are capable of reducing CO_2 in aqueous electrolyte to a promising fuel.

Under Task 2 the team purchased two Gamry Potentiostats. One will be used for an HTE electro polymerization process and the other will be used for an HTE carbon dioxide electrolysis setup. For fuel detection, the team purchased a duel inlet mass spectrometer (includes membrane inlet (MIMS) probe to analyze liquid samples). Additionally, a polisher was purchased to allow reuse of glassy carbon substrates.

Electro polymerization will take place in a JCAP fume hood that has been dedicated for CEC HTE use. Electro polymerization process will be carried out using a Gamry potentiostat. The potentiostat is equipped with a control desktop computer and electrochemistry software (ECHEM200). A mobile rack was purchased to hold the control computer, potentiostat, and auxiliary equipment, which will be placed outside the fume hood. The breadboard base with the electrochemical cell, translation stages, and the fluid supply will be mounted in the fume hood (Figure 6). The potentiostat and ECHEM software were setup and tested on the prototype electro polymerization cell. The electro polymerization process has to be carried out in an oxygen free environment.

Figure 6: Solid Works View of the HTE Set Up

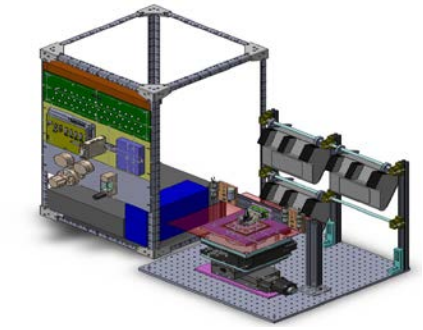

The CO_2RR will be carried out in HTE setup using a Gamry potentiostat. The potentiostat is equipped with a desktop computer and ECHEM200 software (Figure 7) and has been setup and tested on the prototype electrolysis cell. In this configuration, CO_2 gas is be supplied from a gas cylinder to saturate the electrolysis electrolyte solution. This has been setup on a laboratory bench-top provided by JCAP and dedicated to Energy Commission HTE.

Figure 7: HTE Set Up for CO_2 Electrolysis

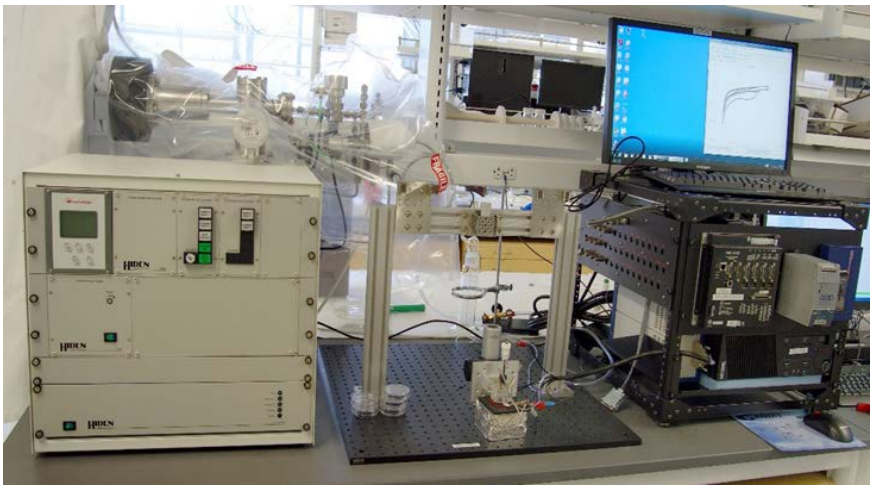

MS instrument on the left; control box on the right with the call platform in the middle.

A Hiden Dual HPR-20 R&D MIMS Gaseous Fuel Detection mass spectrometer was purchased and will be used as the primary analytical tool for fuel detection to support the HTE experimentations. It has been set up and tested. This sophisticated analytical tool will help not only in identification of promising catalysts but also promising candidate fuels. Consequently the instrument will work in conjunction with the HTE electropolymerization tool and enable definition of the synthesis parameters.

Mass Spectrometer instrument is capable of analyzing gaseous products such as H_2 and CO and volatile hydrocarbon products in aqueous solution such as alcohols. The Hiden mass spectrometer is equipment with a MIMS Probe that is capable of analyzing liquid fuel (Figure 8). The stand-alone mass spectrometer will be incorporated in the HTE CO_2 electrolysis setup. The work of Task 4 involves developing software to fully control and synchronize the mass spectrometer with HTE experimentation sequences.

A glassy carbon material was selected as the working electrode substrate and a polishing machine was purchased to remove the deposited films after CO_2RR testing to enable the researchers to reuse valuable glassy carbon material. The polishing machine will substantially reduce the cost of using the glassy carbon material. In summary, the listed equipment has been delivered and is operational. The software to control these devices is being developed.

Figure 8: The MIMS Probe Attached to the Mass Spectrometer

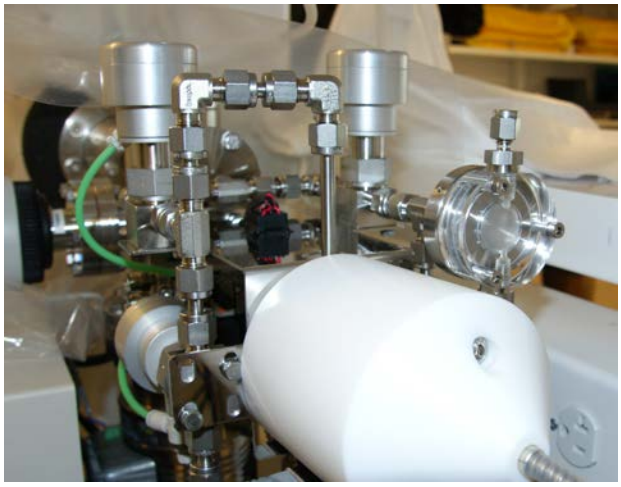

1.1.3 CIT Safety

All personnel are required to be safety-trained prior to starting any work in the laboratories in accordance with institutional safety regulations and procedures. Researchers are safety trained by the laboratory safety officer at Caltech. Before using any chemicals, researchers must consult the material safety data sheet (MSDS) for instruction on handling the material in question. All users are required to use the appropriate personal protection equipment when handling chemicals—this minimum PPE required for most procedures include lab safety glasses, appropriate gloves, and a fire-resistant laboratory coat. Additional PPE may be required as per the Caltech safety policy and materials' MSDS. Energy Commission personnel are required to follow the procedures developed by Caltech for hazardous waste storage and removal. All personnel must review the Caltech provided emergency response guide, which is prominently displayed in every research lab. A more comprehensive list of general safety guidelines can be found in the Caltech Chemical Safety Manual and JCAP Specific Safety Checklist.

1.2 Lawrence Berkeley National Laboratory, Laboratory Readiness

Lawrence Berkeley National Laboratory (LBNL) Task 2 established laboratory setup directed toward CO_2RR research: Tasks 3 and 5. Task 3 focused on the development and optimization of CO_2RR molecular catalysts for liquid fuel production. Task 5 focuses on membrane separation technology for liquid fuel production. The equipment acquired under Task 2 is listed in Table 2.

Table 2: List of Equipment and Instruments

Item description (make and model)	Task #	Location	Vendor	PO#	Price per unit	# of units	Date purchased	Date received	Total Price
APC System (GPC)	5	976 JCAP-LBNL	Waters Technologies	7106594	$87,946.40	1	5/20/14	7/25/14	$87,946.40
Automatic Gas Pycnometer (Piknometer)	5	976-132 JCAP-LBNL	Micromeritics	7109043	$16,355.00	1	6/24/14	8/15/14	$16,355.00
Potentiostat	5	976-132 JCAP LBNL	Bio Logic	517149	$17,552.00	1	6/25/14	8/20/14	$17,552.00
Dew Point Generator (Humidity controller)	5	976-JCAP LBNL	LICOR	518654	$7,601.70	1	7/29/14		$7,601.70
FTIR Spectrometer (ReactIR)	5	976-JCAP LBNL	Mettler-Toledo	228656	$69,054.00	1	7/30/14		$69,054.00
Hybrid Rheometer	5	976-JCAP LBNL	TA Instruments	228669	$58,400.00	1	7/30/14	8/27/14	$58,400.00
Polarimeter	5	976-JCAP LBNL	Rudolph Research Analytical	518695	$5,875.00	1	7/30/14		$5,875.00
Flow controller systems & cell assembly	3	976-132 JCAP LBNL	Alicat Scientific	519513	$8,280.00	1	8/13/14	8/25/14	$8,280.00

1.2.1 LBNL: CO_2RR Molecular Catalysts Laboratory

Two experimental systems were constructed under Task 2 for use in Task 3, as described in this report.

A gas-handling manifold and photo electrochemical cell were designed in conjunction with a SRI gas chromatograph (GC) to establish the ability to perform quantitative measurements of the gas phase and liquid phase products of carbon dioxide reduction. Equipment items were used in the construction of the flow manifold. The schematic of the GC system is shown in Figure 9 and describes the flow controller system, gas purifiers, and the electrochemical cell.

Figure 9: Schematic of GC System Set Up at JCAP, LBNL

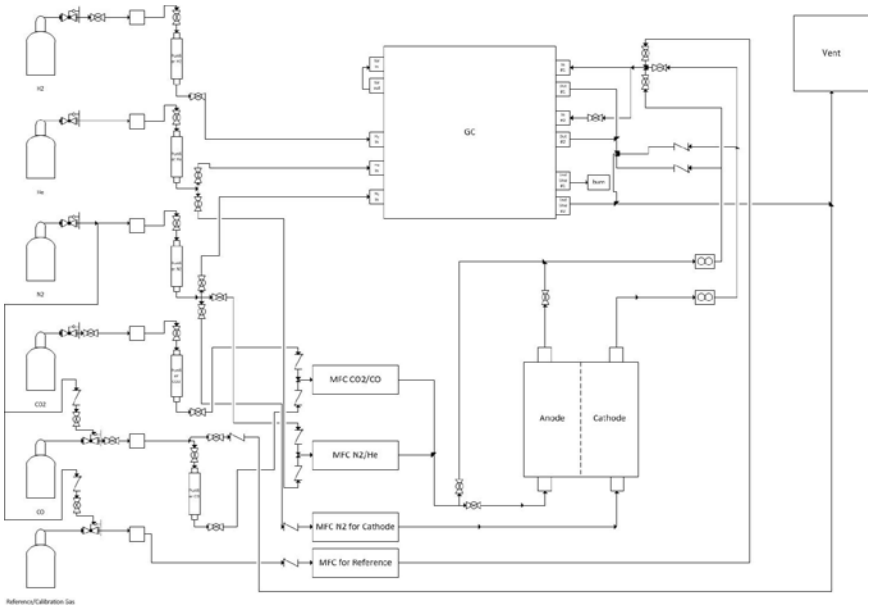

Figure 10 shows the SRI GC connected to the gas handling system. The photo in the middle shows the gas purification system, which is a part of the gas handling system used to produce the high purity gases, which then provide the necessary feed streams for the GC and the electrochemical cell. The picture on the right shows three of the four purchased mass flow controllers. These are used to precisely regulate the flow of gas into the electrochemical cell.

Figure 10: SRI GC System

The top left picture shows the SRI GC connected to the gas handling system. The top right picture shows the gas purification system, which is a part of the gas handling system. The bottom picture shows three of the four mass flow controllers, which were purchased.

A flow cell for CO_2 reduction was designed and fabricated. The design is compatible with electrochemical catalysis and photo electrochemical catalysis. The volume of the cell was minimized to increase the response time and sensitivity for detecting the products of CO_2 reduction. The cell is connected in-line, via the flow manifold, to the GC for the detection of gas phase (H_2, CO, CH_4, C_2H_4, C_2H_6). Samples of the electrolyte are taken at the end of an electrolysis experiment for detection of the liquid products (e.g., methanol, ethanol, propanol, formate, allyl alcohol). The system has been designed to minimize the loss of volatile products like the alcohols during the electrolysis when gas is flowing so that they can be accurately quantified in the off-line detection scheme.

Figure 11 shows a chromatograph depicting the detection of gas phase products of CO_2 reduction. Figure 12 depicts what the typical CO_2 reduction efficiency results from the system. In this experiment, a test catalyst showed the reduction of CO_2 to H_2, ethylene, methane, and CO.

Figure 11: Read Out of the Signal from the GC for a Calibration Gas

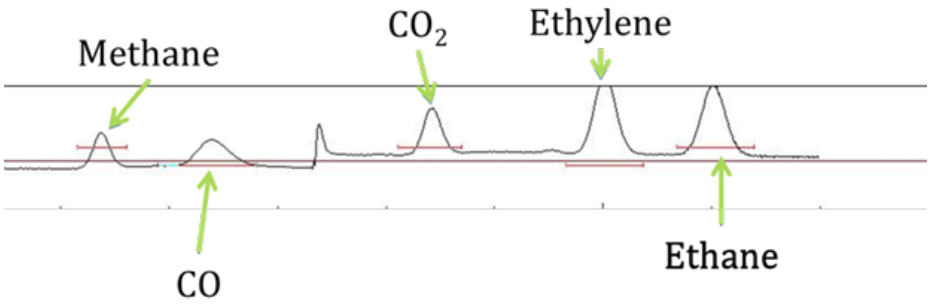

Calibration gas containing 50 ppm of methane, carbon monoxide, carbon dioxide, ethylene, and ethane.

A gas chromatograph cycle takes approximately 30 min to complete. The need to obtain repeated measurements, for accuracy, and to evaluate catalyst stability leads to a typical run of six hours. The system is designed to run unattended and can be monitored remotely. The practical limit for evaluation of catalysts with the system is 2-3 per day. Higher throughput would be possible by running a number of CO_2RR cells in parallel with parallel gas chromatographs.

Figure 12: Experimental Measurements of the Faradaic Efficiencies for H_2, Ethylene, Methane, and CO for a Model Cu-Containing Electrocatalyst

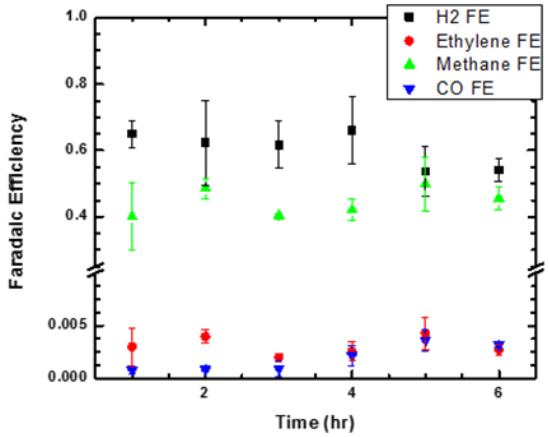

The high-pressure liquid chromatograph (HPLC) was installed (Figure 13). The HPLC instrument is designed to detect liquid phase products of CO_2 reduction, e.g., formate, methanol, ethanol, etc.. With the combination of gas phase chromatography and high-pressure liquid chromatograph, all of the expected products of CO_2 reduction can be measured quantitatively and at high sensitivity.

Figure 13: Photo of the High-Performance Liquid Chromatograph (HPLC)

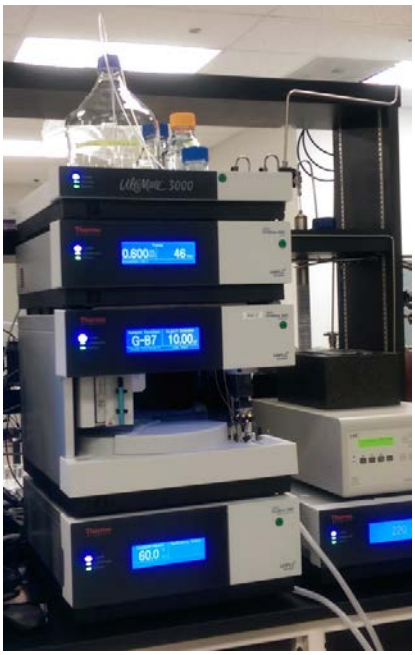

The HPLC is operating and is capable of separating all liquid phase CO_2 reduction products, i.e., glycolaldehyde, formic acid, formaldehyde, acetaldehyde, methanol, allyl alcohol, ethanol, 1- or 2-propanol (Figure 14).

Figure 14: Chromatogram of Peak Separations from the Installed HPLC

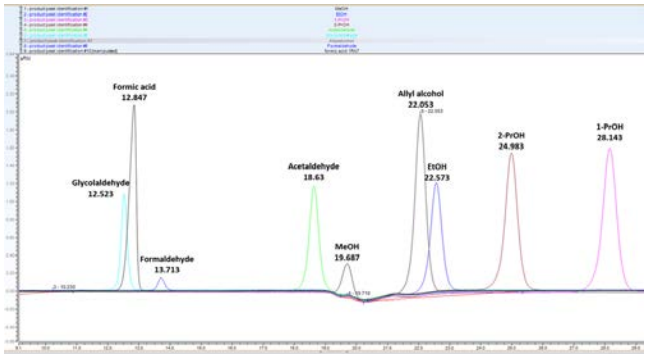

The column installed in the HPLC is Aminex HPX-87H, which is packed with H-exchange resin, is running with 0.5 mM H_2SO_4 as eluent at 60 ˚C column oven temperature. The detection limit of the expected products is defined by the sensitivity of the UV-Vis and a refractive index detector (RID) detectors to be on the order of 1~10 µM. The maximum throughput of the HPLC system is 48 samples per day. In summary, all equipment and laboratory are operational.

1.2.2 LBNL: Membranes Laboratory

LBNL has established a Membrane Research Laboratory focused on accelerating research in membranes for the electrocatalytic reduction of carbon dioxide. To accomplish its mission, the

membranes group at JCAP has acquired the equipment under Task 5. The summary of the instrumentation functionality and applications follows.

Gel permeation chromatograph (APC System) by Waters Technologies, Inc. was installed. The team has been trained and is currently using the APC system for routine characterization of molecular weight of polymeric membrane precursors (Figure 15). The rheometer has been installed, and used to measure melt-viscoelasticity (polymer dynamics), which is important in understanding the transport of diluents across polymer films, as well as ascertaining mechanical properties of thin film samples, such as those used to make membranes (Figure 16).

Figure 15: Gel Permeation Chromatograph

Credit: Waters Technologies, Inc.

Figure 16: Rheometer

Credit: TA Instruments, Inc.

Polarimeter by Rudolph Research Analytical was purchased to study the materials made in the course of new membrane discovery that use precursors that are stereo chemically defined

either at the monomer or polymer level. The instrument provides an additional necessary method of measuring optical rotation, indicative of the presence of a single enantiomer or isotacticity. The potentiostat by BioLogic, Inc. is used by the membranes group for the routine measurement of ionic conductivity (one impedance channel), and the electrochemical measurement of oxygen concentration for permeability (Figure 17).

Figure 17: Potentiostat

Credit: BioLogic, Inc.

Additionally, the team is sharing this instrument with the molecular catalyst researchers. Polymer density may be directly coupled to the permeability of neutral species across polymeric membranes. The automatic pycnometer enables the determination of polymer density, which will vary as the degree of crystallinity in the proposed material is also changed (Figure 18).

Figure 18: Automatic Gas Pycnometer

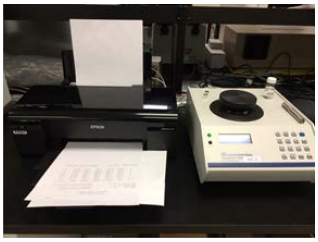

Credit: Micrometrics

In situ FTIR spectroscopy provides a powerful tool for quantitatively analyzing time-resolved processes, such as permeation of fuel across a polymeric membrane, and polymerizations used to make membrane precursors (Figure 19) and is used in Task 5 research activities.

Figure 19: FTIR Spectrometer in Situ

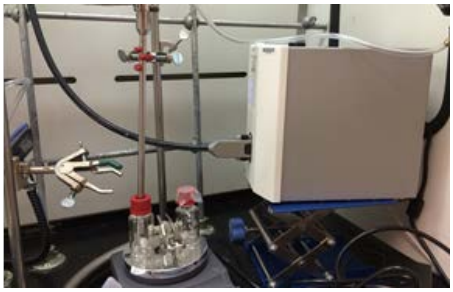

Credit: Mettler-Toledo

Many of the operating environments for the membrane may be in a vapor-fed device. Controlled humidity is a requisite to understand transport of fuel across experimental films. Dew Point Generator by LICOR, Inc., was purchased to conduct that research activity (Figure 20). In summary, all the equipment and laboratory are operational.

Figure 20: Dew Pont Generator

Credit: LICOR, Inc.

1.2.3 LBNL Safety

All of the personnel are safety trained according with institutional safety rules and procedure. The Energy Commission researchers at JCAP range broadly in level of experience and scientific discipline. A system of safety work leads ensures there is appropriate supervision and training in safe practices, and a safety technician assists with compliance and resolution of issues as they arise. The Safety Committee, which comprises safety leads for each laboratory sector and is chaired by a Berkeley Lab Staff Scientist, meets monthly to work on safety improvements. The Operations Manager Kristin Estis is the Safety Officer for JCAP at Berkeley Lab.

CHAPTER 2:
Task 3: Expand Efforts in the Development and Optimization of CO2RR Molecular Catalysts for Liquid Fuel Production

2.1 Polymer Coordination Promotes Selective CO_2 Reduction by Cobalt Phthalocyanine

2.1.1 Introduction

Selectively reducing CO_2 into fuels using molecular catalysts is an important strategy to develop renewable energy sources. Molecular catalysts have been reported to form a single, typically 2-4 e^- CO_2 reduction products.[1-17] Cobalt phthalocyanine (CoPc) is a molecular CO_2RR catalyst.[18-26] It can be adsorbed to graphite electrodes reducing CO_2 to CO in aqueous solution with co-generation of H_2. Previous studies have shown that incorporating CoPc into a poly-4-vinylpyridine (P4VP) membrane increases the catalysts selectivity for the production CO from CO_2 over the evolution of H_2 from water,[27-28] however the exact mechanisms for the enhanced activity and selectivity is not defined. Two properties of P4VP may contribute to the enhancement of catalysis. First, individual pyridine residues can coordinate to the square planar cobalt center of CoPc, and second, the uncoordinated pyridine residues, which form the secondary and outer coordination spheres of CoPc, may contribute to the increased activity. It was important to determine how P4VP increases the activity and selectivity of CoPc for CO_2 reduction, because this knowledge can help in the designs of improved immobilized molecular CO_2RR catalyst systems for wider applications of solar-fuels technology.

The properties of P4VP are assessed independently to determine how each affects CO_2RR by CoPc. Electrodes modified with CoPc and CoPc-P4VP were studied using controlled potential electrolysis (CPE) to better understand the base activity of the catalyst itself and the increase in activity that coincides with P4VP encapsulation. The CoPc-P4VP system was found to be among the most active molecular catalyst reported for the selectively reducing CO_2 to any single product in aqueous solution.[28-26] To investigate the influence of axial coordination in the absence of the polymer film, electrodes modified with axially coordinated CoPc(py) were prepared from deposition solutions of CoPc in the presence of pyridine. Likewise, to separate the intrinsic properties of the polymer from axial coordination effects, electrodes with four-coordinate CoPc, and five-coordinate CoPc(py) encapsulated in a non-coordinating poly-2-vinylpyridine (P2VP) membrane were prepared (Figure 21). The results suggest there is a synergistic relationship between axial coordination and the chemical environment imposed by the P4VP membrane that leads to dramatic enhancements in activity observed for CoPc-P4VP.

Figure 21: Proposed Molecular Structures of CoPc, CoPc-P4VP, CoPc(py), CoPc-P2VP and CoPc(py)-P2VP

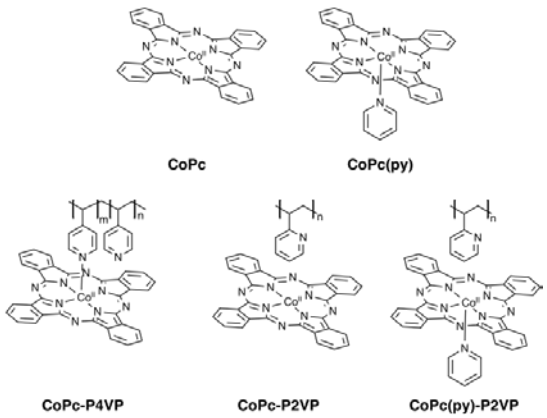

2.1.2 Results and Discussion

Electrodes modified with CoPc and CoPc-P4VP were prepared to investigate the CO_2RR catalytic activity of the free catalyst and the effect of the P4VP support. Details of the experimental work can be found in (Kramer and McCrory, 2016, doi: 10.1039/C5SC04015A). Cobalt phthalocyanine is known to be a competent HER (Hydrogen Evolution Reaction) catalyst.[37-40] Under an atmosphere of N_2, scans negative of the phthalocyanine reduction show the onset of a catalytic wave attributed to HER at approximately –1.04 V vs. SCE (Saturated Calomel Electrode) for CoPc modified electrodes and –1.08 for electrodes modified with CoPc-P4VP. Under a CO_2 atmosphere, the onset of the catalytic wave shifts positive for both films (Figure 22).

Figure 22: Representative Cyclic Voltammograms of (left) CoPc and (right) CoPc-P4VP Under N_2 and CO_2

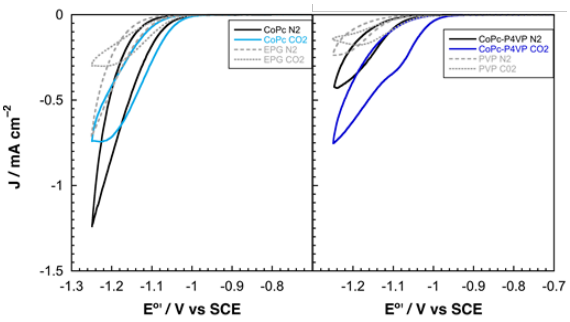

To ensure steady state delivery of substrate to the electrode surface, the researchers performed rotating disk electrode voltammograms (RDEVs) finding that CoPc-P4VP displays much greater peak currents than CoPc (Figure 23). The more negative onset potential for H_2 evolution with CoPc-P4VP modified electrodes suggests that the P4VP film suppresses hydrogen generation compared to free catalyst. The onset of the catalytic wave under CO_2 was not affected by the presence of the polymer film indicating that P4VP does not similarly suppress CO_2RR activity of CoPc.

Figure 23: Representative Rotating Disk Electrode Voltammograms at 1600 RPM

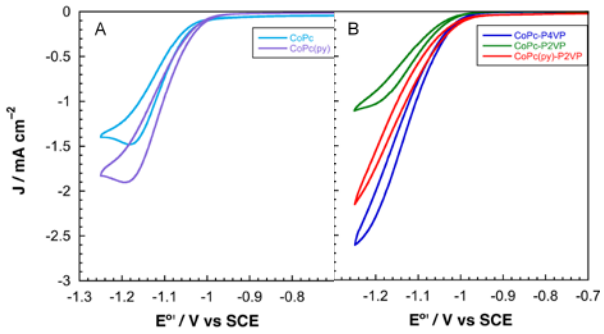

A) the free catalysts CoPc (light blue) and CoPc(py) (purple) and B) polymer immobilized catalysts CoPc-P4VP (dark blue), CoPc-P2VP (green) and CoPc(py)-P2VP (red) under an atmosphere of CO_2.

To assess Faradaic efficiencies for CO_2 reduction by CoPc and CoPc-P4VP, researchers performed experiments at –1.25 V vs SCE (Table 3). The only products observed for both films were CO and H_2.

Table 3: Results from 2 h CPE Experiments at –1.25 V vs SCE for CoPc Modified Electrodes

	Charge / C	ε_{CO}	TON_{CO} (2h)	TOF_{CO} (s^{-1})	ε_{H2}	ε_{total}
CoPc	**0.58 ± .24**	**36 ± 7%**	**$4.5 \pm 2.4 \times 10^3$**	**0.6 ± 0.3**	**41 ± 8%**	**77 ± 10%**
CoPc(py)	**0.83 ± .48**	**68 ± 3%**	**$1.2 \pm 0.7 \times 10^4$**	**1.6 ± 1.0**	**19 ± 5%**	**87 ± 6%**
CoPc-P4VP	**1.9 ± 0.20**	**89 ± 3%**	**$3.4 \pm 0.4 \times 10^4$**	**4.8 ± 0.6**	**5 ± 1%**	**94 ± 3%**
CoPc-P2VP	**0.36 ± .08**	**73 ± 8%**	**$5.6 \pm 1.8 \times 10^3$**	**0.8 ± 0.2**	**12 ± 3%**	**85 ± 9%**
CoPc(py)-P2VP	**1.76 ± 0.27**	**83 ± 5%**	**$3.0 \pm 0.5 \times 10^4$**	**4.2 ± 0.7**	**6 ± 5%**	**89 ± 7%**

The reported values are averages of measurements from at least three experiments with independently prepared electrodes. Errors are given as standard deviations except for those for ε_{total} which were calculated as standard errors.

To investigate the influence of axial coordination on CO_2RR activity of CoPc in the absence of the polymer film, electrodes modified with the pyridine coordinated catalyst, CoPc(py). RDEVs of the CoPc(py) films under an atmosphere of CO_2, at 1600 rpm, display a positive shift in the onset potential of the catalytic wave, compared to CoPc, and a significant increase in the peak catalytic current over the parent complex. During two hour electrolysis experiments, CoPc(py)

films passed ~1.5 times more charge than CoPc, with average current of 0.96 mA cm^{-1}Faradaic efficiencies for CO with CoPc(py) were more than double the parent catalyst at 68%.

To separate the secondary and outer coordination sphere effects of the polymer membrane from the axial coordination effects, modified EPG electrodes were prepared with CoPc encapsulated in a poly-2-vinylpyridine (P2VP) membrane. RDEVs of CoPc-P2VP under CO_2 show the onset of catalysis at potentials similar to CoPc, with peak currents lower than those of the parent catalyst. CoPc-P2VP films passed much less charge during the electrolyses than CoPc-P4VP. However, CoPc-P2VP operated with ε_{CO} = 73%, much higher than CoPc. Compared to CoPc, CoPc- P2VP showed practically identical TON_{CO} and TOF_{CO} during the two hour electrolyses. These experiments indicate that while the P2VP support does not increase the activity of CoPc for CO_2 reduction, it does suppress evolution of hydrogen.

Electrodes modified with CoPc(py) dispersed in a P2VP membrane (CoPc(py)-P2VP) were prepared to reintroduce the axial ligand to CoPc in the P2VP catalysts films. Incorporating a more active, five-coordinate CoPc catalyst in the P2VP film increased CO_2RR activity by nearly an order of magnitude. The onset potential of CO_2RR catalysis in RDEVs of CoPc(py)-P2VP occurred at nearly the same potential as CoPc-P4VP with similar peak currents. Faradaic efficiency for CO was increased from 73% without pyridine, to 83%. By reintroducing an axial ligand to CoPc in P2VP the CO_2RR performance was restored to the level observed for CoPc-P4VP.

By itself, CoPc is an unremarkable CO_2RR catalyst that displays poor selectivity and relatively low activity for CO_2RR. Once immobilized in P4VP, the selectivity for CO production jumps to nearly 90% with close to an order of magnitude increase in the TON_{CO}. In fact, CoPc-P4VP is among the most active and selective molecular CO_2 reduction catalysts yet studied in aqueous solutions. Its high activity and selectivity are notable, even in comparison to heterogeneous catalysts like copper,[42-47] and gold (Table 4).[46,48,49] Our work showed that the P4VP membrane alters the chemical environment of the catalyst to promote the reduction of CO_2. The ability of P4VP to coordinate CoPc and the coordination sphere effects are the major contributors to the increased activity (Figure 24). The detailed discussion analysis of the roles of the axial ligands, primary and secondary coordination effects of the catalytic activity and selectivity can be found in Kramer and McCrory, 2016, doi: 10.1039/C5SC04015A.

In summary, immobilization of cobalt phthalocyanine in poly-4-vinylpyridine dramatically improves its activity as a catalyst for reducing CO_2. The polymer membrane was shown to slow down the competing hydrogen evolution reaction, while enhancing the rate of CO_2RR compared to the polymer-free catalyst. The CoPc(py) and CoPc-P2VP results show that neither the primary, secondary or outer coordination sphere effects alone are responsible for the large increases in CO_2RR activity. These effects must be combined to produce highly active and selective catalysts.

Table 4: Results from Two Hour CPE Experiments at –1.25 V vs SCE and RDE

Catalyst	Activity / mA cm^{-2}	V vs RHE	pH	Products (ε)	TOF / s^{-1}	Ref
CoPc-P4VP	2.0 ± 0.2	-0.73	4.7	CO (89 ± 3 %), H_2 (5 ± 1%)	CO: 4.8	this study
CoPc(py)-P2VP	1.9 ± 0.2	-0.73	4.7	CO (83 ± 5 %), H_2 (6 ± 5%)	CO: 4.2	this study
CoPc-(90% P4VP, 10% STY)/BPG	NR	-0.7	4.4	CO (71.6%), H_2 (21.0%)	CO: 3.1[b]	34
CoPc-(90% P4VP, 10% STY)/BPG	NR	-0.66	6.8	CO (77.2%), H_2 (16.6%)	CO: 2.9	34
[Mn(bpy(tBu)$_2$)(CO)$_3$Br]/ Nafion/MWCNT	1.8	-0.75	7	CO (46%), H_2 (44%)	CO: 0.002	37
Ni(cyclam)-PALA	NA	-0.17	8	CO (92%)	CO: ~ 0.002	38
Poly(Cr(vinylterpy)$_2$)	NR[d]	-0.52	5.8[e]	HCHO (87%)	NR	39
Re[(bpy)(CO$_3$)Br]/Nafion	0.002	-0.65	7	HCO_2H (48%), CO (16.5%), H_2 (39%)	CO : 0.002, HCO_2H: 0.006	40
Co(Ch)/MWNT	NR	-0.83	4.6	CO (89%)	CO: 0.04	41
Ir-Pincer (2^{MeCN})	0.60	-1.0	6.95	HCOOH (93%), H_2 (7%)	NA (7.3 s^{-1})	42
Ni(cyclam)	0.64-0.97[f]	-0.67	5	CO (84 ± 4%)	NA	43
Ni(MTC)	0.64-0.97[f]	-0.67	5	CO (88 ± 7%)	NA	43
Ni(MCC)	0.64-0.97[f]	-0.67	5	CO (92 ± 2%)	NA	43
Ni(HTC)	0.64-0.97[f]	-0.67	5	CO (88 ± 7%)	NA	43

Kinetic measurements for CoPc modified electrodes. Errors are given as standard deviations except for those for ε_{total} which were calculated as standard errors.

a) Solution phase catalyst at 20 mg/mL concentration. B) These TOF values were recalculated from the literature report using the total loading of catalyst cast onto the surface (1 x 10-10 mol cm-2), as opposed to the amount detected by CV (5 x 1012 mol cm-2). Researchers believe using the total amount of catalyst deposited provides a more accurate comparison to other reported values in the literature. C) Calculated from the electrolysis data provided in the report (79% FE for CO, 1.69 C passed in 24h) and the estimated catalyst concentration based on the 2 mg mL–1 concentration of the catalyst-modified polymer. D)No time information was provided for the electrolysis in the report, so activity and TOF could not be calculated for the electrolysis. However, the reported Koutecky-Levich analysis in the manuscript yields a TOF of 5.2 s-1. eEstimated pH of 0.1 M NaClO4 saturated with CO2.

Figure 24: Illustration of CoPc Immobilized in P4VP

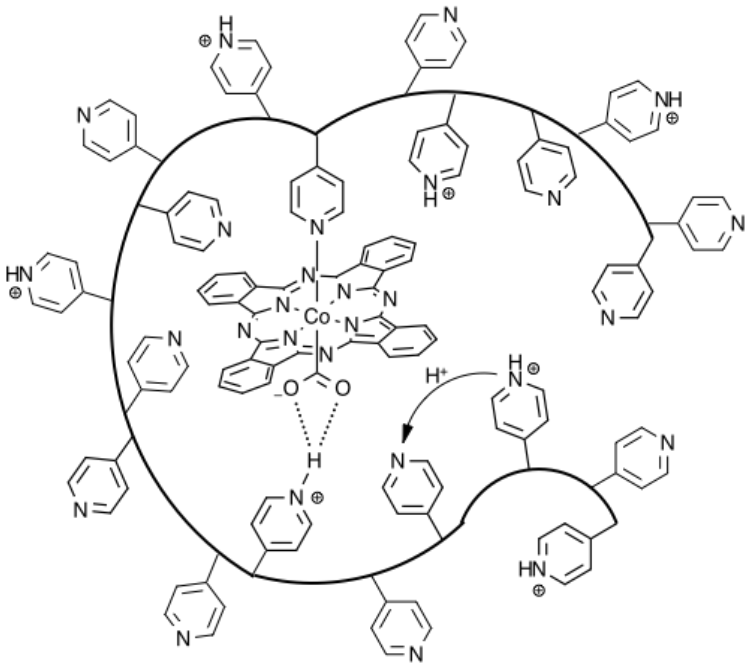

Three properties of the polymer membrane which are suggested to be important to the activity and selectivity of CoPc-PVP are illustrated. Pyridine residues that can coordinate to CoPc, the ability for uncoordinated pyridine residues to act as proton relays, and the hydrogen bonding interactions that may occur between protonated pyridines and activated CO_2.

2.2 Immobilization Study of Carbon Dioxide Reduction Catalyst on Electrode Surface

2.2.1 Introduction

To examine the ability of molecular catalytic systems to perform reactions under realistic operating conditions of a fuel-generating device, immobilization of these systems on the electrode surfaces was investigated. Electrodes with immobilized molecular catalysts are good candidate structures for the conversion of CO_2 to fuels and other high commodity chemicals. There are several approaches to immobilizing catalysts on the surface – the team studied the noncovalent interactions as means of stably attaching the molecular catalysts to the surfaces of the electrode. Specifically, researchers designed, synthesized, and characterized a manganese (I) tricarbonyl catalyst (**1**) for CO_2 reduction to CO that features appended pyrenyl carboxamide groups that can drive association with graphitic carbon surfaces.

2.2.2 Results and Discussion

High-resolution XP spectra collected for samples of **1** on high-surface area carbon electrodes suggest the presence of intact **1**, as well as a second species. The spectral features suggest the possible presence of decomposed, Mn^{2+}-containing material as the identity of the second species. Pronounced satellite features in Mn 2p spectra at high binding energy are consistent with a species having unpaired spin in the valence levels. Mn^{2+} is a good candidate proposal, as

prior work has demonstrated that the 3s response in Mn^{2+} species is split by the exchange interaction energy of the unpaired 3d spins and the 3s electron remaining following X-ray photoionization from the 3s level.

Consistent with the presence of multiple species on the electrode surface, selectivity was attenuated in this system versus a homogeneous, purely molecular analogue. Production of CO gas was successfully measured with high Faradaic yields, but some production of H_2 gas was also measured. This result is consistent with a mechanistic proposal involving selective CO_2 reduction at the intact manganese(I) tricarbonyl sites, and H_2 production at the less well defined secondary sites.

2.3 Investigation of Carbon Dioxide Reduction with Low-Valent Low-Coordinate Iron and Cobalt Complexes

2.3.1 Introduction

The syntheses of formally zero-valent two-coordinate iron and cobalt complexes was successfully developed.[1] These are unusual complexes that could only be obtained utilizing a combination of steric and electronic stabilization provided by an unique carbene ligand, namely a cyclic (alkyl)(amino)carbine.[2] The synthesis of these complexes was achieved by reductive complexation, followed by halide abstraction and a final one-electron reduction yielding complexes of iron **1** and cobalt **2** (Figure 25).

Figure 25: Synthesis of Zero-valent, Two-coordinate Iron and Cobalt Complexes

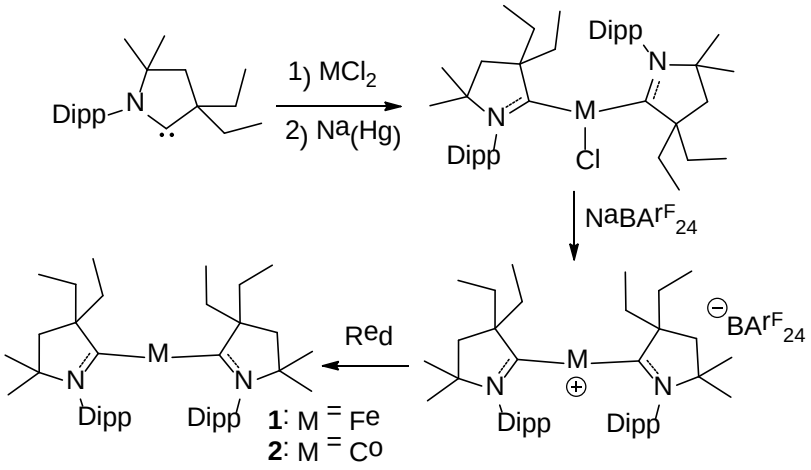

The complex **1** was able to bind dinitrogen at low-temperature and activate it in the presence of a reductant (Figure 26). This result prompted us to assess its viability as a catalyst for dinitrogen reduction utilizing proton sources and electrons. It was shown at very low temperature (-95 °C), complex **1** is a competent pre-catalyst for the generation of super-stoichiometric amounts of ammonia (up to 4.6 equivlant per catalyst).[3]

Figure 26: Reduction of Dinitrogen Using a Two-coordinate Iron Complex

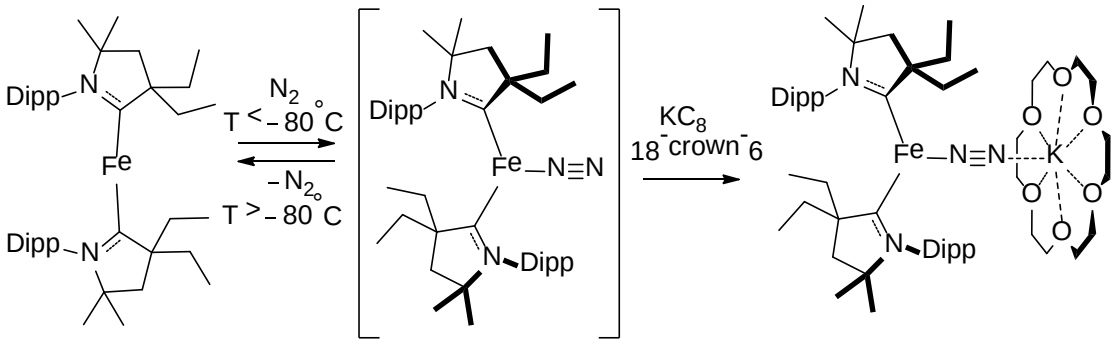

Because of the remarkable activity of complex **1**, researchers investigated the possibility of catalytic reduction of CO_2 using protons and electrons, chemically and electrochemically, with the same complexes **1** and **2** systems.

2.3.2 Results and Discussion

The electrochemistry of complexes **1** and **2** were investigated under an atmosphere of CO_2. Both complexes feature a reversible reduction event around -2.1 V vs. Fc/Fc^+ (Figure 27 left) under a dinitrogen atmosphere; however, in the presence of CO_2, several electrochemical events appear with no tractable catalytic waves (Figure 27 right). This result prompted us to investigate the reaction of the complex with carbon dioxide without application of a current.

Figure 27: Cyclic Voltamograms of Complex 1

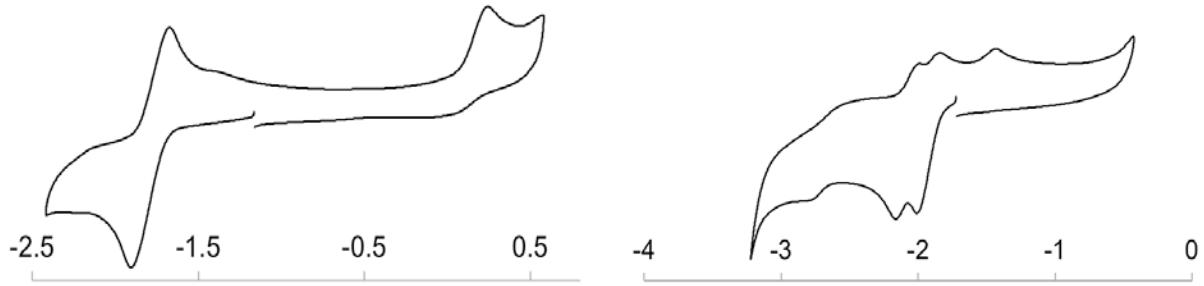

High-resolution XP spectra collected for samples of **1** on high-surface area carbon electrodes suggest the presence of intact **1**, as well as a second species. The spectral features suggest the possible presence of decomposed material, as the identity of the second species. Pronounced satellite features in Mn 2p spectra at high binding energy are consistent with a species having unpaired spin in the valence levels. Mn^{2+} is a good candidate proposal, as prior work has demonstrated.

Reaction of complexes **1** and **2** under an atmosphere of CO_2 yielded rapid color change of the reaction mixture from dark green to colorless and deposition of black precipitate assigned to elemental iron and cobalt, respectively. The content of the solution was intractable utilizing standard spectroscopic techniques. The amount of CO_2 used during the reaction was reduced to

only stoichiometric amounts. For complex **1**, the same decomposition was observed; however, with complex **2**, a notable change of color from dark green to dark red was observed. After several minutes, black elemental cobalt started to deposit, indicating some degree of decomposition. The reaction was monitored by infrared and electron paramagnetic resonance spectroscopies. In Figure 28, the incorporation of an activated CO_2 moiety in the complexes (1661 cm^{-1}) was observed by IR.

Figure 28: Infrared Spectrum of the Reaction of Complex 2 with Stoichiometric CO_2

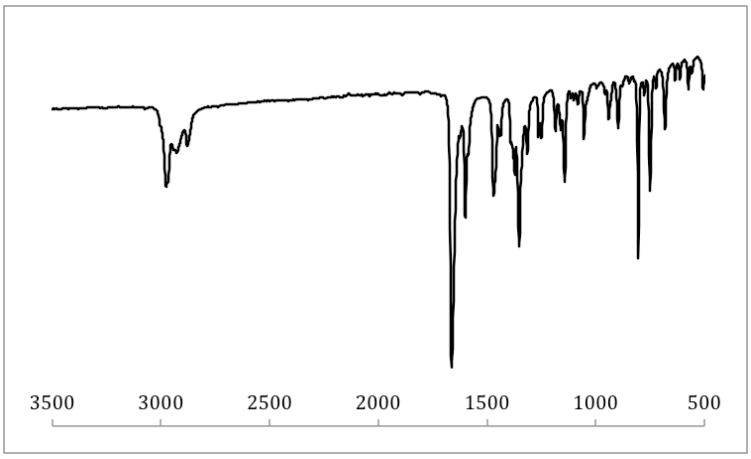

By EPR spectroscopy (Figure 29), at early time points using a freeze-quench technique, the remaining starting material and a new species can be observed; which parameters seem to indicate the presence of an organic radical fragment which does not interact with the transition metal center.

Figure 29: EPR Spectrum of the Reaction of Complex 2 with Stoichiometric CO_2

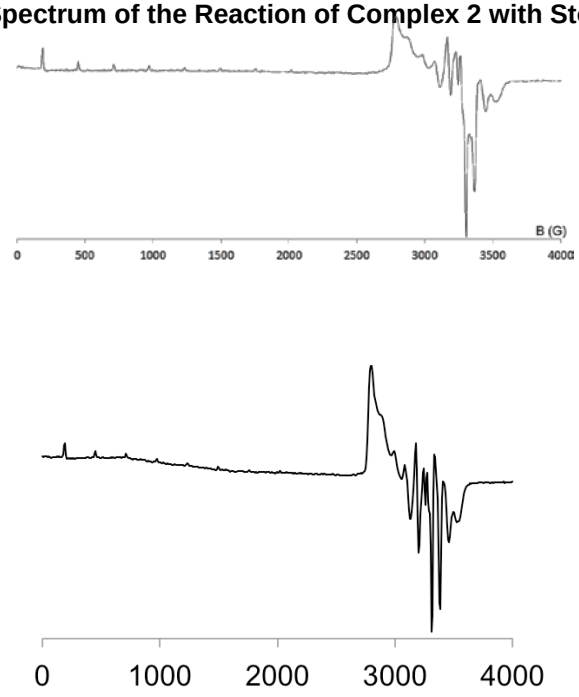

Top) authentic sample of complex 2 for comparison; bottom) freeze-quenched sample at two minute time point.

As mentioned earlier, the reaction of complex **2** with stoichiometric amounts of CO_2 eventually leads to precipitation of elemental cobalt (Figure 30). Analysis of the supernatant by NMR and EPR spectroscopies revealed the presence of a radical species.

Based on these results, it was hypothesized that the initial reaction of complex **2** with carbon dioxide generates an inserted CO_2 complex **3,** which slowly decays to the organic radical **4** along with loss of elemental cobalt. The mass recovery does not fit with the stoichiometry, indicating either an incomplete reaction or decomposition of the starting material.

Figure 30: EPR Spectrum of the Reaction of Complex 2 with Stoichiometric CO_2 After Cobalt Precipitation

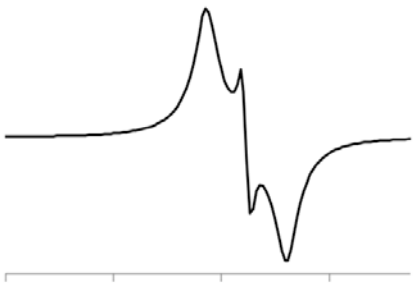

In summary, the study found new complexes (0-valent 2-coordinate Fe/Co complexes) as potential pre-catalysts for CO_2 reduction and formulated a hypothesis of the reaction mechanism. The initial results are positive. However, further examinations of the stoichiometry

and optimal operation environment is still required to determine their efficiency of reduction and viability.

2.4 Effects of Local Environment of the Electrochemical Reduction of CO_2

2.4.1 Introduction

Heterogeneous catalytic electroreduction of CO_2 by noble metals leads to mixtures of products, and only Cu can produce hydrocarbons. In all case H_2 formation competes with CO_2 reduction. In this chapter is described an evaluation of several types of molecular modifications of the catalytic environment on noble metal electrodes. The hypothesis was that these modifications could potentially result in improved selectivity for reduction products, suppression of H_2 formation, and increased reduction efficiency by controlling the way in which CO_2 interacts with the catalytic surface.

2.4.2 Results and Discussion

Carbon is a good support for Cu nanoparticles because it is electrically conducting. While there have been many reports in the literature on using carbon-supported Cu, the results of these studies are not consistent. Motivated by recent evidence that carbon supports contain substantial amount of metallic impurities, experiments were conducted to establish the role of these impurities.[1] To this end, several commercially available carbon supports were obtained, leached in ultra-pure nitric acid, after which the acid was analyzed to determine the metal content. These experiments revealed that all of the supports contain metals (e.g., Fe, Mn, Co) at ppm levels. In the presence of these metals the supports exhibited electrochemical activity for CO_2 reduction to CO and H_2, and when Cu was present to CH_4. However, after leaching of the metal impurities, all of the supports exhibited the similar low current densities and only produced H_2. An additional finding of this work was that electrochemically deposited Cu nanoparticles exhibited 5-fold higher activity for the formation of CH_4 than independently produced Cu nanoparticles dispersed onto the same support. These findings suggest that electrodeposition of Cu occurs at defects in the carbon support, which enhance the electrocatalytic properties of Cu. The exact mechanism of the enhancement in activity is not understood and would require additional effort to establish.

Amine groups are known to react with CO_2 to form carbamates and it was, therefore, reasoned that the attachment of amine groups to a carbon support would enhance the availability of CO_2 to Cu nanoparticles supported on the carbon. To this end, amine groups were grafted onto carbon nanotubes free of impurities. After grafting, the amount of amine groups on the nanotubes was about 2.9wt% amine. Cu nanoparticles (10 nm in diameter) were prepared by a colloidal method and then dispersed onto the amine-treated carbon nanotubes. Long-term electrolysis at a fixed applied potential (-0.9 V vs. RHE) was carried out for Cu nanoparticles supported on carbon nanotubes (Cu-CNT) and on carbon nanotubes containing grafted amines (Cu-EDA-CNT).

Figure 31 compares the current densities and Faradaic efficiencies for these two catalysts. It is evident that the grafting of amine groups onto carbon nanotubes produces a slight increase in the overall activity of Cu nanoparticles at any potential and alters the Faradaic efficiency in favor of producing formic acid, instead of CO or H_2 at low small potentials, but at larger negative potentials, Faradaic efficiencies of Cu-EDA-CNT and Cu-CfNT become comparable. Subsequent analysis has shown that the observed differences between the two catalysts are not consistent with the original premise that the amine groups would enhance the local concentration of CO_2 in the vicinity of the Cu nanoparticles. Instead, the amine groups may serve as local pH buffers that keep the pH from rising as the magnitude of the negative applied potential is raised.

Figure 31: Current Densities and Corresponding Faradaic Efficiencies for CNT-EDA-Cu and CNT-Cu

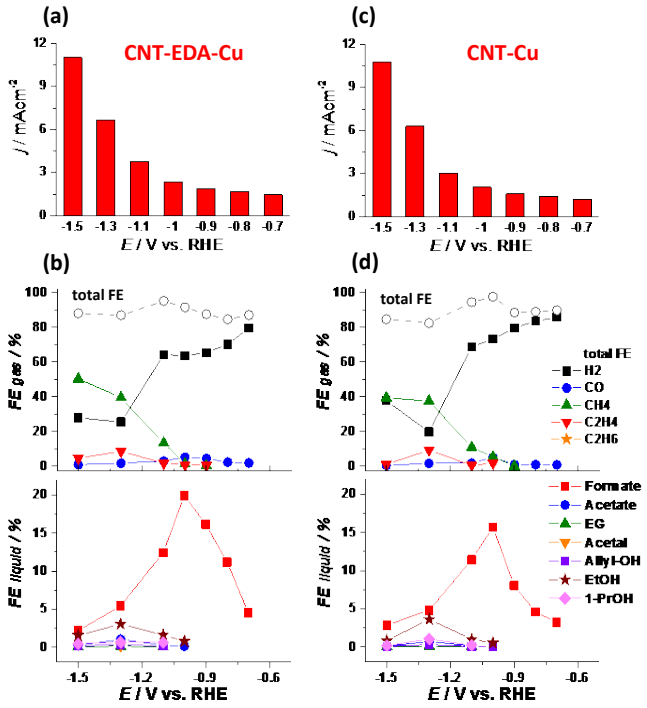

Gaseous products (upper panels) are H_2, CO, CH_4, C_2H_4 and C_2H_6 and liquid products (lower panels) are formic acid, acetic acid, ethylene glycol (EG), acetaldehyde (Acetal), allyl alcochol (Allyl-OH), ethanol (EtOH), and 1-propanol (1-PrOH). Data points for gaseous products are obtained by averaging four successive analyses by gas chromatography and the liquid products are collected at the end of the electrolysis and analyzed by high performance liquid chromatography.

A conceptually novel approach for designing CO_2RR catalysts has been explored. This *de novo* catalyst design makes use of surface modification of extended heterogeneous CO_2RR catalysts with discrete molecular elements as a tool, to modulate the catalytic activities of those catalysts. As shown in Figure 32, researchers have successfully prepared a series of group 11 metal electrodes (Cu, Ag, and Au) modified with cucurbituril molecules of different sizes (CB[n]; n denotes the number of the repeating units and can be 5, 6, 7, or 8). The binding of these cyclic molecules to metal surfaces, characterized by XPS, features “mutidentate” interaction

between the carbonyl groups of CB[n] and the metal surfaces. The hydrophobic cavities of CB[n], depending on their sizes, can capture different number of CO_2 molecules inside, and, therefore, should enrich CO_2 at the electrode surfaces and favor the reduction of CO_2 over H_2O. It was found that, for example, the CB[5]/CB[8]-modified Au electrodes, compared to bare Au electrodes, exhibitited increased Faradeic yields of CO and decreased Faradaic yields of H2, by approximately 10%.

Figure 32: CB[n]-modified Group 11 Metal Surfaces for CO_2RR and New Catalytic Architectures

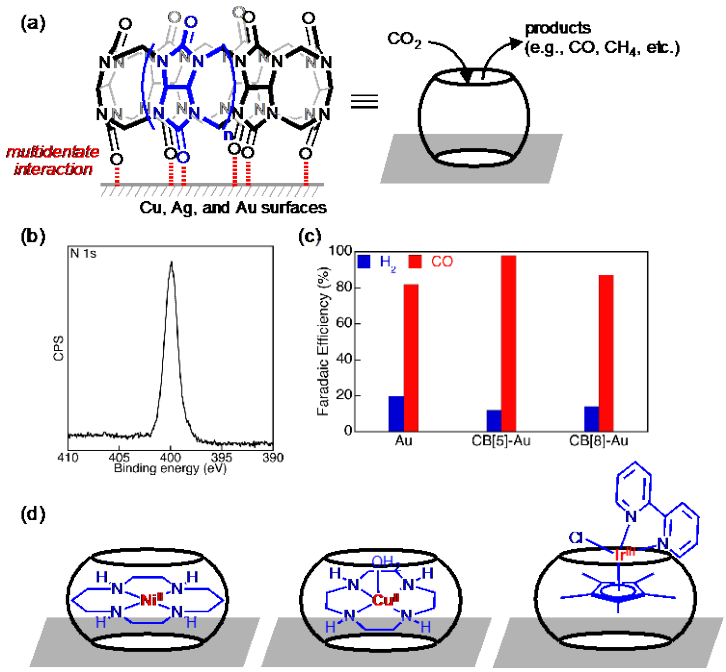

Architectures featuring molecular complexes confined within CB[8] and on metal surfaces.

Relying on the rich supramolecular chemistry of CB[n], three host-guest complexes were prepared between CB[8] and three different metal complexes (Ni(cyclam), Cu(cyclen), and Ir(bipy)Cp*Cl_2), and further demonstrated the immobilization of these host-guest complexes onto the surfaces of group 11 metals. The possibility of introducing a metal complex into the cavities of the surface-bound CB[8] opens up an additional space for catalyst discovery, where cooperative effects between the surface-confined metal complex and the metal surface could be envisioned and, potentially, be utilized for designing novel CO_2RR catalysts.

The electrochemical activity of CB[8] containing Ni(cyclam) and Ir(bipy)Cp*Cl_2 for CO_2 reduction has been undertaken. The initial results show that Ni(cyclam) is not stable. XPS analyses made before and after electrolysis reveals that the Ni is leached out of the cavity of CB[8], very likely as nickel carbonyl ($Ni(CO)_4$). By contrast, the Ir in Ir(bipy)Cp*Cl_2 is retained. Experiments are under way to identify the products formed by CB[8] containing Ir(bipy)Cp*Cl_2.

The findings of this work is presented in Table 5. The results show that discrete molecular modifications of catalytic electrode surfaces do not provide a facile means of affecting the

catalytic reactions in contrast to the membrane incorporation approach described in Section 2.1.

Table 5: Reaction Conditions Evaluated

Support	Catalyst	CO_2 reduction activity
Carbon supports	none	none
Carbon supports	Metal impurities	CO + H_2
Carbon nanotubes	Cu nanoparticles	Liquid, gas reduction products
Carbon nanotubes	Cu nanoparticles + amines	Small changes compared to amine-free case
Au	Cucurbituril [5 or 8]	CO + H_2, with H_2/CO reduced compared to pure Au
Au	Cucurbituril[8] + Ni cyclam	unstable
Au	Cucurbituril[8] + Ir(bipy)Cp*Cl_2)	Not tested

2.5 Detection of Electrochemical Reduction of CO_2

The initial phase of the project was devoted to the design and construction of an electrochemical cell for evaluating catalysts, as well as the assembly of the necessary analytical capabilities for determining products formed in the gas and liquid phases. The electrochemical cell was designed to assure good mass transfer from gaseous CO_2 entering the cell as bubbles to the electrolyte, so as to maintain saturation of the electrolyte throughout an experiment. This capability was essential to avoid undesired mass-transport effects near the cathode of the cell where CO_2 reduction occurs. This goal was achieved by embedding a glass frit at the bottom of the cell, which was capable of producing bubbles 0.2 mm in diameter. The volume of electrolyte in the cell chosen to be small (1.8 mL in each chamber) to reduce the time required to accumulate products that are soluble in the electrolyte.

Figure 33 shows schematic drawings of the cell used to evaluate electrocatalysts. The cell is fed by a continuous flow of CO_2 and the gaseous products leaving the cell are analyzed by a gas chromatograph (GC, SRI multigas #3). Products that are soluble in the electrolyte are accumulated over the period of 30-60 minutes and then analyzed by high performance liquid chromatography (HPLC). The potential applied to the cell is controlled by a Biologic VSP-300 potentiostat. To evaluate catalyst performance, the cell potential was fixed and the effluent gases were sampled every 20 minutes, corresponding to the cycle time of the GC, and the liquid products were sampled at the end of the run. If it was desired to determine the effects of applied potential on the total current through the cell and the composition of all products, the preceding procedure was repeated for a series of fixed potentials. Data from either mode were then analyzed and the results reported as the current density for the chosen applied potential

and the product Faradaic efficiency. The latter quantity gives the fraction of the total current passed through the cell that is used to produce a specific product.

Figure 33: CO2 Reduction Electrochemical Cell Composed of an Anode and Cathode Chamber

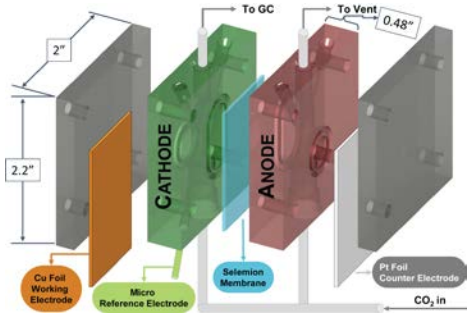

Chamber separated by an anion-conducting memberane. Schematic of the apparatus for evaluating electrocatalysts. Reprinted from Lobaccaro, P. et al. Effects of Temperature and Gas-Liquid Mass Transfer on the Operation of Small Electrochemical Cells for the Quantitative Evaluation of CO2 Reduction Electrocatalysts. Phy. Chem. Chem Phys., DOI: 10.1039/C6CP05287H (2016).

CHAPTER 3:
Task 4: High Throughput Screening Capability for Ligands

3.1 Carbon Fuels and the Need for High Throughput Screening

3.1.1 Introduction

A critical technology for enabling solar-based generation of liquid fuels is the selective reduction of CO_2 to an energy-carrier molecule. Liquid fuels comprise a range of molecules that are combustible, and a particularly attractive example of a liquid fuel that may be synthesized via CO_2 reduction is methanol. Ethanol is another promising liquid fuel as well as fuels such as methane, ethane, propane and butane that are not liquid at ambient conditions but can be easily liquefied for adoption into existing fueling technology and infrastructure, as has been done for LPG (liquefied petroleum gas). Another critical technology area for solar fuel generation is the engineering of device architectures that efficiently couple light harvesting components to catalysts that perform fuel synthesis reactions, such as the conversion of CO_2 to methanol.

Inspecting the status of these two critical technology areas reveals the need for developing a new high throughput screening capability. The science of CO_2 reduction is most typically performed using molecular catalysts in which a catalyst molecule is designed to interact with a CO_2 molecule, a proton source, and an electron source to convert these reactions into, for example, a methane molecule. The molecular catalyst is generally dissolved in solvent to create a homogeneous catalyst system in which the ability to design and control the reaction process on the molecular level is the basis for scientific endeavors and often involves the use of specific proton and electron sources. These reaction conditions are quite different from the ones utilized in advanced solar fuels devices, which typically (1) use water as a proton and electron source, (2) do not contain non-aqueous solvents, and (3) require the catalyst to be adhered to a solid-state surface for direct coupling with the light harvesting components of the device. These three differences between basic research in molecular catalysis and device engineering comprise a substantial barrier to the development of solar fuels technology, and research efforts to bridge these gaps have had limited success to date.

To accelerate technology transfer from molecular homogeneous catalysis to solar fuel generators, the focus of Task 4 was to develop a high throughput experimental capability to translate basic scientific research to deployable device components. Given the operational differences noted above, the high throughput pipeline requires two primary instruments: a “Combinatorial Electro-Polymerization System” (CEPS) that enables synthesis of solid-state catalyst electrodes and a “Combinatorial Fuel Detection System” (CFDS) to identify the catalyst electrodes that produce fuels of interest. The CEPS operates in non-aqueous solvents in which many molecular catalyst precursors are dissolvable and the CFDS operates in aqueous

electrolytes per the standard designs of solar fuel generators. As such, these two systems operate in different environments and require different approaches to instrument design, yet for deployment of high throughput screening they must operate in conjunction with compatible formats of catalyst electrodes. The design, fabrication, and testing of these systems have been successfully completed and are described in the following two chapters. For further details on the catalyst systems, their performance, and the rates of fuel production, please see the Chapter 2 of this report.

3.1.2 Combinatorial Electro-Polymerization System

In addition to meeting the practical requirement that the catalyst must be synthesized as a solid electrode, catalyst electro-polymerization enables incorporation of additional species that may promote if not directly participate in the catalytic cycle, such as CO_2-binding or electron-conducting species. An optimal catalyst electrode may therefore contain multiple components whose optimal loadings and concentrations are not known. To facilitate rapid exploration of the synthesis parameter space, combinatorial strategies can be employed, motivating the development of an electropolymerization cell with automated solution handling and potentiostatic control to systematically vary parameters in an array of catalyst samples on a library plate. Since the electropolymerization solutions generally contain non-aqueous solvents, the solution handling components must be fabricated from chemically resistant materials and operated in a fume hood. A photograph of the system for meeting these stringent requirements is shown in Figure 34, which also includes a schematic of the custom-designed and built electropolymerization cell.

Figure 34: Combinatorial Electro-Polymerization System

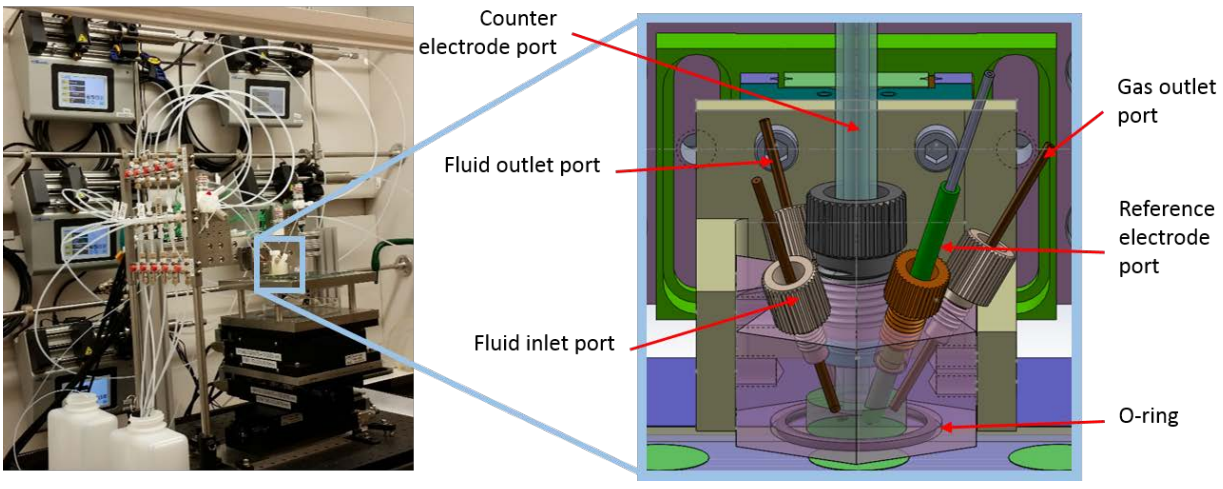

Photograph of the CEPS in a fume hood with the various motion and solution handling components (left). Catalyst synthesis occurs in the small cell noted by the blue box. (right) A schematic drawing of the cell is shown with the various ports labelled and the schematic catalyst samples represented by green circles on the library plate.

This miniature electrochemical cell houses a variety of ports required for solution handling and controlling the electrochemical environment with the same fidelity as traditional techniques.

While a researcher employing traditional synthesis techniques can typically produce 1-4 electropolymerized catalyst electrodes per day, the CEPS is designed to synthesize 25 catalyst electrodes in a single run, and since multiple runs can be performed in a day with a single operator the experiment rate is increased by more than 10-fold.

The miniature electropolymerization cell and automated cell positioning system enables automated synthesis of an array of catalyst electrodes, which is depicted as an array of unique colored samples in Figure 35. This figure also shows representative data acquired using the CEPS, where the redox characteristics of an electropolymerized catalyst exhibit the same properties as catalysts synthesized by a laborious manual procedure.

Figure 35: Electropolymerized Catalyst Library

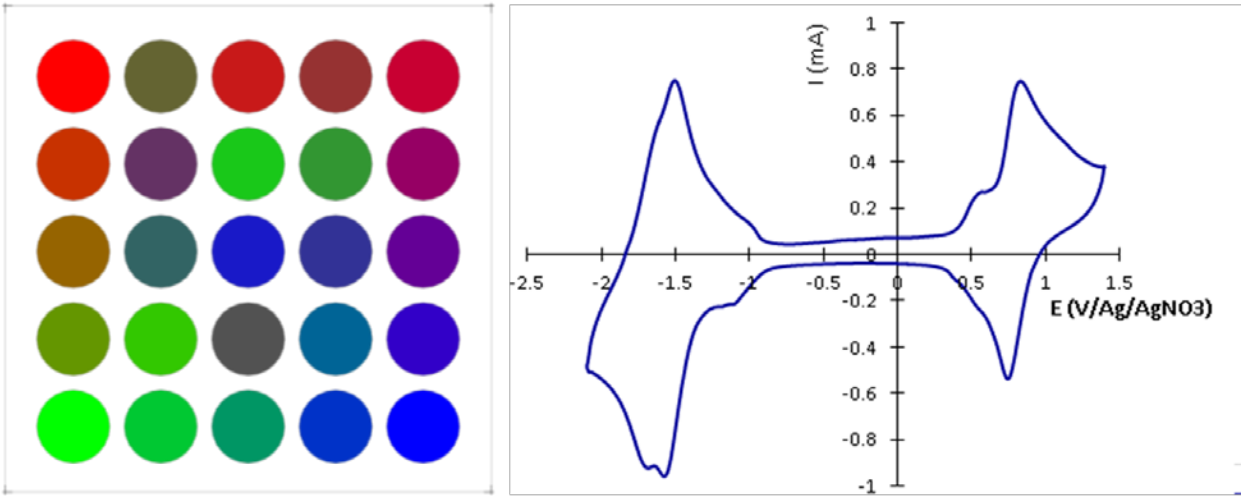

(Left) A schematic of a catalyst library containing an array of catalyst spots, which are indicated by colored circles, whose color indicates a unique property; in this case the red:blue:green ratio indicates the designed ratio of complex A:complex B:polymer precursor in the electrodeposition solution. (Right) An electropolymerized Fe(v-trpy) catalyst film synthesized through electroreduction in the custom CEPS cell. The pairs of oxidation and reduction waves in this example CEPS data demonstrate that the Fe catalyst complex was successfully synthesized using the high throughput technique. Credit: California Institute of Technology

3.1.3 Combinatorial Fuel Detection System

A catalyst library synthesized in the CEPS must be evaluated using a combination of electrochemical and analytical chemistry techniques to ascertain whether this electrode produces products of interest for a solar fuels generator. The CFDS performs automated fuel production and detection experiments on the catalyst libraries. Since ambient conditions and aqueous electrolytes are desirable for a deployable technology, the CFDS operates under these conditions and was fabricated on a laboratory bench, as shown in Figure 36. The motion control system and cell concept are similar to that of the CEPS with all other components custom designed and built for this application.

Figure 36: Combinatorial Fuel Detection System

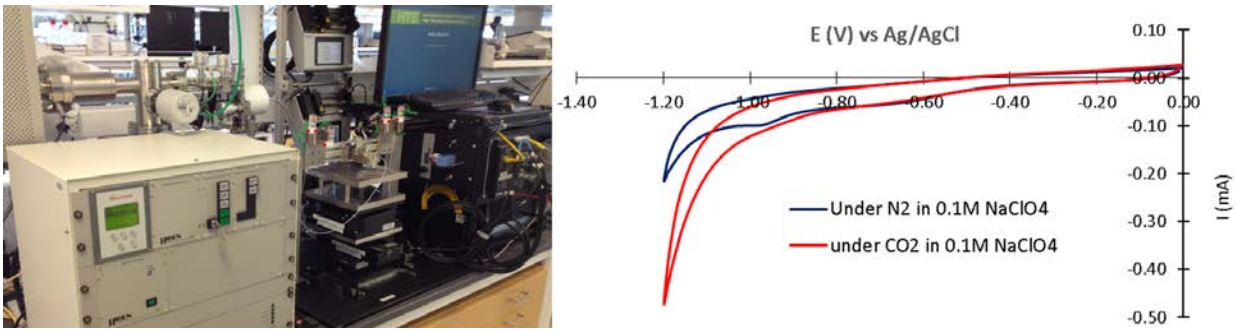

Example CO_2 electroreduction data for the Fe(v-trpy) catalyst film synthesized using CEPS. Thedifference between the red and blue (with and without CO_2 in the cell) is the CO_2 reduction signal.

The electrochemical cell in the CFDS is coupled to a mass spectrometer for detecting gaseous fuels and fuels dissolved or mixed in the aqueous electrolyte at a measurement throughput unattainable with GC or HPLC. This measurement rapidly identifies optimal catalysts but with limited quantification of the fuel products, which serves as rapid dietnfication of the catalysts that warrant more detailed investigation using the traditional techniques described in Chapters 1-2. The fuels are detected according to the associated molecular mass or mass fragment, with larger molecular mass generally corresponding with a more desirable, energy-dense fuel. To track the many molecular masses of interest and automate the solution, motion, and electrochemical components of the experiments, custom software was developed and an example image of the CFDS software is shown in Figure 37 where the many colored traces correspond to different mass spectrometry and electrochemical signals.

Figure 37: A Screenshot of the Custom Software Developed for the CFDS

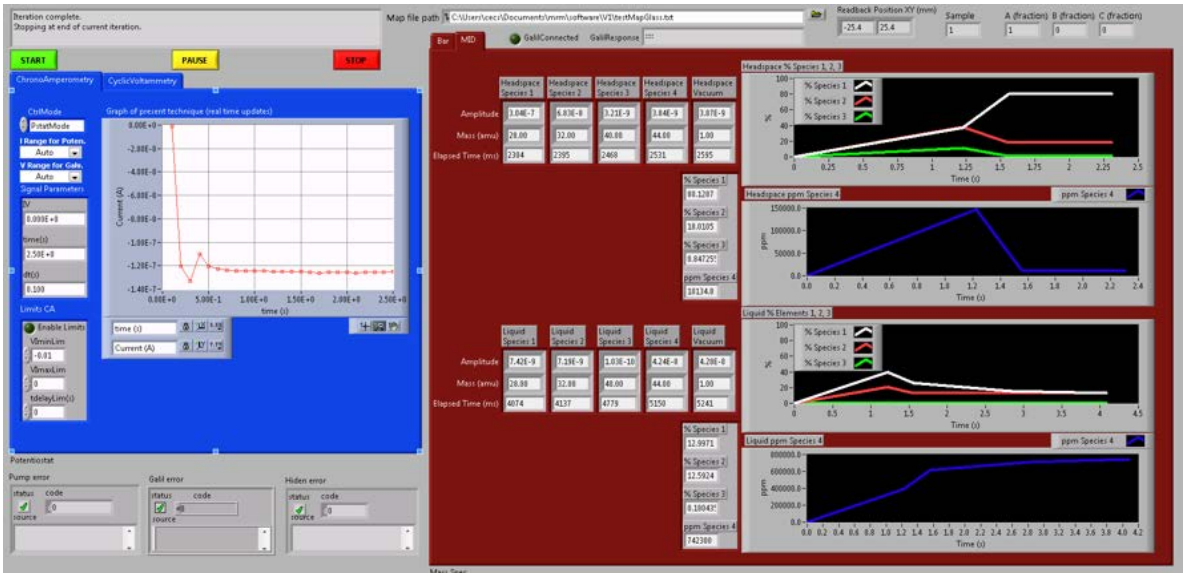

Screenshots shows mass spectrometry signals for quantifying fuel production.

The mass spectrometer itself is a commercially available instrument, and the invention that enables the CFDS to operate is the electrolysis cell that provides research-grade electrocatalysis data, can be automatically rastered across a catalyst library, and is coupled to the mass spectrometer with automated switching between detection of gas and liquid fuels. A detailed schematic of the cell is provided in Figure 38. The cell contains three ports for electrode contacts and three ports for liquid and gas handling and a single port for coupling to an electropolymerized catalyst sample:

A. Working electrode port including pressure sealing of the cell to a catalyst electrode using an o-ring gasket

B. Counter electrode port. The tube shown in port B terminates in the testing solution with a partition to separate the counter electrode and working electrode solutions while maintaining ionic communication.

C. Reference electrode port in which a standard electrochemical reference electrode is inserted into the testing solution.

D. Gas filling port through which the cell atmosphere can be filled to a controlled composition and pressure

E. Liquid filling port through which solution is inserted into the cell to contact all 3 electrodes and initiate an experiment

F. Gas aliquot port through which gas (containing electrochemically-produced gaseous fuel) can be extracted and delivered to the mass spectrometer

G. Liquid aliquot port through which liquid (containing electrochemically-produced liquid fuel) can be extracted and delivered to the mass spectrometer.

Figure 38: Custom Electrolysis Cell for Catalyst Testing

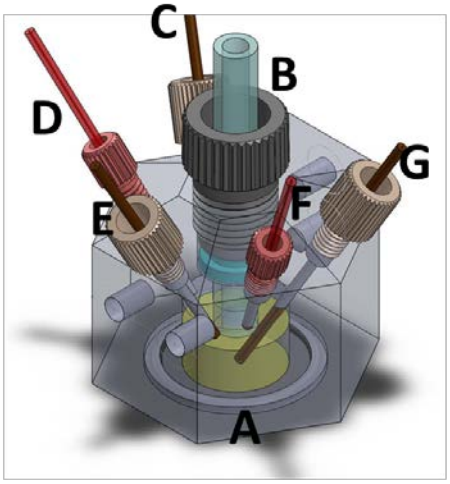

A schematic of the electrolysis cell for the CFDS showing the seven ports integrated into a miniaturized cell that can be readily coupled to a fuel detection instrument.

The solution flow from port E to port G can vary from continuous (e.g., to create a flow cell with time-resolved product detection) to intermittent (e.g., to perform bulk electrolysis measurements). All ports are sealed to maintain control of the atmosphere within the cell. Stage motors move a library plate of catalysts to perform an automated series of measurements.

The combinations of the CEPS and CFDS comprise the first high throughput-screening platform for assessing which molecular catalysts can be readily integrated into a solar fuels generator. This technology bridges the science-engineering gap and accelerates technology development for renewable generation of fuel.

CHAPTER 4:
Task 5: Development of Membranes and Separation Technology for Liquid Fuel Production

4.1 Introduction

Membranes are a key element of a device that converts sunlight to fuels because they separate products, inhibit back reactions at the electrodes that reduce efficiency, and conduct ions required for operation as illustrated in Figure 38.

Figure 39: Schematic of Device to Convert CO2 to Liquid Fuels

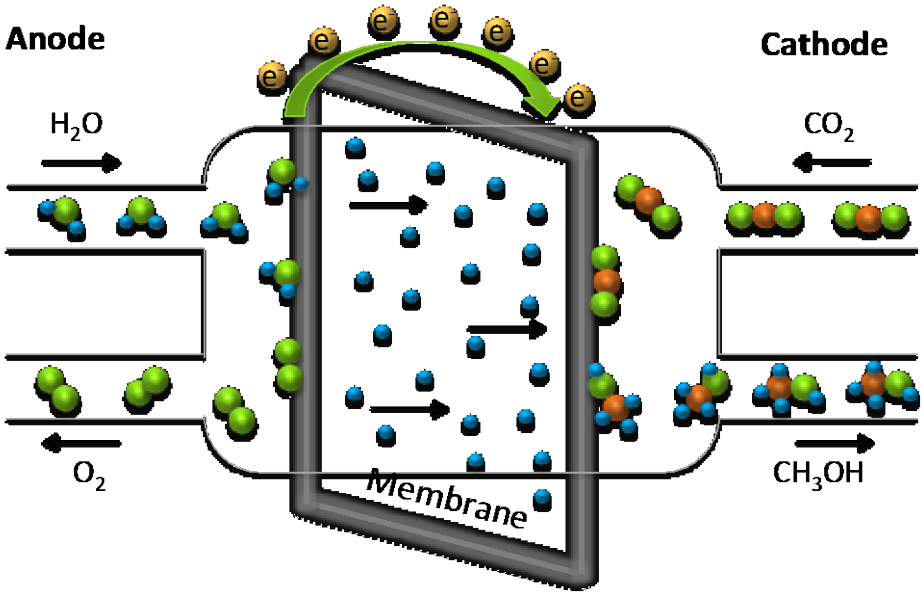

Illustration of fluidic elements of a photoelectrochemical CO_2 device (photoelectrocatalytic structure is not shown for clarity). On the anode side, water is oxidized to generate protons (blue) that are used to reduce CO_2 on the cathode side to hydrocarbon products. Protons pass through the membrane, which blocks crossover of CO_2 (present as bicarbonate in aqueous solution) and methanol.

Robust membranes for solar water splitting applications to make H_2 are available both from commercial sources and advanced research programs. No such membranes exist for conversion of CO_2 to liquid fuels, such as alcohols, alkanes and alkenes. The key challenge is that hydrocarbons and alkanols readily penetrate and plasticize existing membranes, compromising their functions. Solar CO_2 devices are under active development, however, the optimal design characteristics such as composition of the electrolyte, pH, and nature of the primary products are not yet fully defined. Therefore a dual strategy has been used in this work:

(1) design of new architectures that will be sufficiently stable in the presence of hydrocarbons by selecting elements that are mechanically rigid, and therefore limit permeation and swelling by organic molecules, and have ionic character, providing electrical pathways for selective passage of either positive or negative ions. A general design concept is shown in Figure 39.

(2) development of new methodologies to enable synthesis of the membranes and testing of their properties in the presence of organic permeants dissolved in solution. This includes new efficient techniques to optimize conditions for successful synthesis, theoretical investigation of permeation physics, and the first application of Fourier transform infrared spectroscopy to enable real-time studies of solubility and diffusivity of molecules in single and multi-component solutions. These methodologies did not exist previously and are essential for successful development of membranes for solar fuels applications.

Figure 40: General Polymer Membrane Architecture

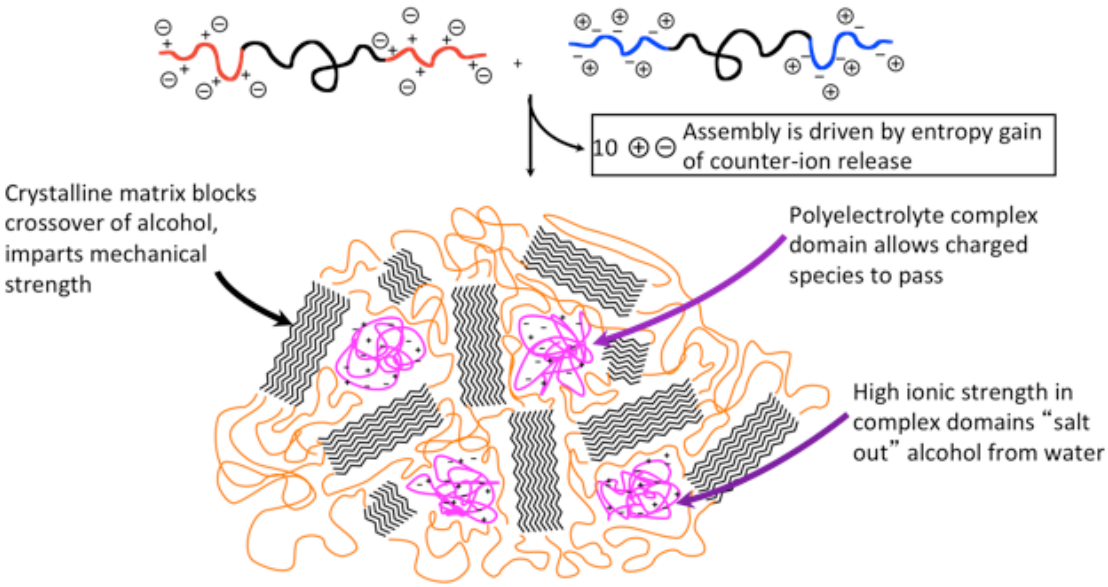

The proposed membrane structure is a blend of copolymers that have desired properties that work together to block product crossover while allowing ions to pass.

4.2 New Membrane Architectures

The major synthetic challenge in developing polymers that are impermeable to organic solvents is finding conditions that enable the polymer chains to remain in solution during synthesis, have the desired molecular structure, and grow to a chain length that ensures good mechanical properties. Several synthetic strategies for the structure in Figure 4.2 were examined for polymerized epoxides that are expected to have the desired blocking and conducting properties via formation of crystalline regions, and be highly tunable. An alternative, randomly crosslinked polymer approach was also investigated. This architecture uses crosslinking rather than crystallinity to confer rigidity and therefore product-blocking properties.

4.2.1 Synthesis of New Membrane Materials via Vandenberg Catalysis

Efforts to synthesize new membrane materials of the type previously shown focused on the ring-opening polymerization (ROP) of mono-substituted epoxides. While allyl glycidyl ether and phenyl glycidyl ether (Figure 40) were used most prominently, approximately a dozen different substituted epoxides were also successfully polymerized in the course of this work.

Polyethers had molecular weights up to 800 kg/mol and a structures ranging from crystalline to gel-like. The extremes – crystalline or gel – do not make useful membranes because of poor mechanical properties. Polymers of butadiene monoxide, tetra-butyl glycidyl ether, butyl glycidyl ether, 1,2-epoxy butane, 1,2-epoxy hexane, 1,2-epoxydodecane, did not forum suitable films for membrane characterization. Polymers of glycidol and propylene oxide were intractable and therefore were not pursued as membrane materials. Styrene oxide and furfural glycidyl ether polymers had low molecular weights and existed as highly viscous fluids, unsuitable for membrane formation.

Figure 41: Ring Opening Polymerization of Allyl Glycidyl Ether (A) and Phenyl Glycidyl Ether (B)

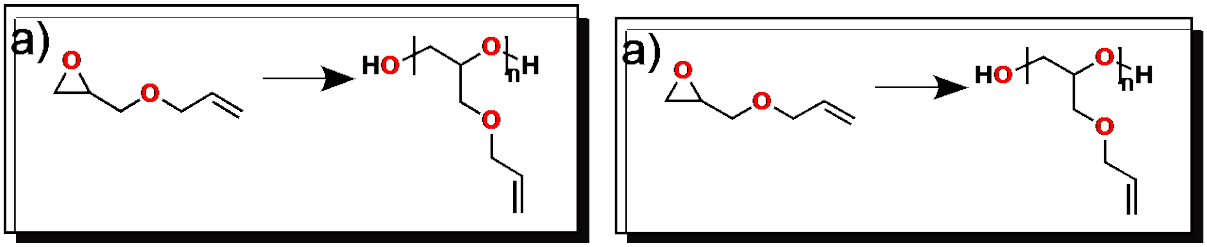

Although allyl glycidyl ether was polymerized into material that could be formed into films, the films were not hydrolytically stable and would therefore not be suitable for solar fuels devices operating with aqueous electrolyte. Poly(phenyl glycidyl ether) PPGE showed particular promise for membranes. Work focused on tailoring the synthesized polymer *via* the enantiomeric composition of the phenyl glycidyl ether feed. As a result of the attachment of the phenyl glycidyl side chain to the planar three membered ring – the core of any epoxide – phenyl glycidyl ether has two distinct enantiomeric forms that can be utilized to tune physical properties. While the synthesis of a racemic mixture of both enantiomers yields an amorphous material, the isolation and subsequent synthesis of the pure enantiomers results in a highly crystalline material.

Membranes were prepared from these materials using standard hot-compression techniques. A series of PPGE membranes were prepared with varying enantiomer content and their gas permeabilities (oxygen, nitrogen and carbon dioxide) were determined wherever possible. Permeabilities were found to be typical for amorphous polymers, in the range of 10^{12} cm^3 cm cm^{-2} s^{-1} Pa^{-1}. However, to the high crystallinity and therefore brittleness of many of these materials under membrane testing conditions accurate and systematic determination of their molecular characteristics proved futile and thereby limited what could be learned of their structure-property relationships.

4.2.2 Synthesis of New Membrane Materials via Anionic Polymerization

A second approach, anionic polymerization, was used to synthesize polymerized epoxides. Anionic polymerization is a standard polymer synthesis method described in many text books that enables formation of chains of well-controlled length. Homopolymers of the crystalline moiety were prepared demonstrating that this component could block methanol transport as effectively as Teflon. Work toward the end of the contract period focused on developing a copolymerization synthesis using synthesis using isomeric mixtures of phenyl glycidyl ether monomers, which have chiral centers that could be further functionalized with ionizable moieties. Control of chirality can introduce flexible blocks that ensure good mechanical properties for membrane fabrication. The synthetic design for these copolymeric materials proved to be challenging, because addition of the second monomer tended to cause premature chain termination and hence polymers of low molecular weight forming membranes with poor mechanical properties. Further research is required to achieve the advantages of this polymer family.

4.2.3 Poly(2,6-dimethyl phenylene oxide) Based Membranes

As an alternative to introduction of controlled crystallinity, membranes that use random crosslinks to introduce product-blocking characteristics have been developed. A series of cross-linked poly(2,6-dimethyl phenylene oxide) (PPO)-based anion exchange membranes containing charged 2-methyl imidazolium groups using a reactive-blending strategy have been synthesized by mixing two PPO-based reactive polymer precursors, one with 20 mol% benzyl-bromide on repeat units, and another containing 20–100 mol% 2-methyl imidazole functional groups. The quaternization and cross-linking reactions occurred simultaneously. The conductivities of those membranes in aqueous solution could reach as high as 87 mS/cm while maintaining a low water uptake (λ <9). For comparison, Nafion's conductivity is in the same range with high water uptake (λ~14). Higher water content is associated with higher product crossover. In aqueous solution, the H_2 permeability of our PPO-based cross-linked membranes is about 1/4 that of un-pretreated Nafion 117 membrane and the methanol permeability is one order of magnitude less than that of un-pretreated Nafion 117. An electrolysis device assembled with PPO-based membrane had similar performance to the device running with Selemion membrane, though the conductivity of Selemion membrane is higher. Importantly, the PPO-based membranes possess better stability than the Selemion membrane in alkaline solution.

4.3 New Methodologies

4.3.1 Improved Understanding of Copolymerization Kinetics

To control the properties of polymeric materials, it is important to understand how the polymer synthesis affects the microstructure of the resultant polymer chains. The most prevalent technique to prepare polymers with multifaceted properties is by copolymerization of two or more monomers. It is crucial to understand how the relative reactivity of each monomer influences the formation of microstructures within the polymer chains, as shown in Figure 41.

Figure 42: Four Copolymerization Microstructures; Random, Gradient, Blocky, Alternating

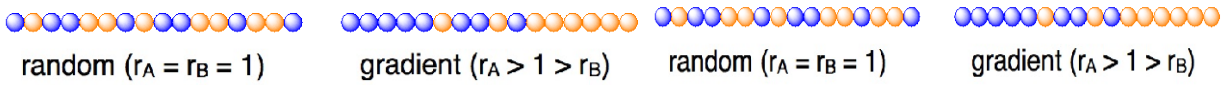

A new methodology to determine copolymerization reactivity ratios was developed and published. This methodology is based on the interactions between the polymer chain ends and the polymerizing monomers. New equations were derived to determine the reactivity ratios for copolymerizations from a single copolymerization experiment. For the copolymerization of two monomers, both reactivity ratios (r_A and r_B) are obtained using Equations 1 and 2; where P_{AB} is the total copolymer conversion, p_A and p_B and individual monomer conversions and n_A is the mole fraction of initial A monomers ($n_A = A_0/(A_0+B_0)$).

$$P_{AB}(p_A) = 1 - n_A(p_A + 1) - (1 - n_A)(p_A + 1)^{r_B} \quad \text{(Equation 1)}$$

$$p_{AB}(p_B) = 1 - n_A(1 - p_B)^{r_A} - (1 - n_A)(1 - p_B) \quad \text{(Equation 2)}$$

Ongoing efforts are focused on examining the copolymerization kinetics of ethylene oxide and allyl glycidyl ether. The polymer synthesis is performed with an FTIR spectroscopy probe submerged in the polymerizing mixture. From the obtained absorption spectra, the relative composition of both monomers is monitored, yielding the kinetics data shown in Figure 42. The data are fit with Equations 1 and 2 to determine the copolymerization reactivity ratios.

Figure 43: Copolymerization Total Conversion as a Function of Monomer Conversion

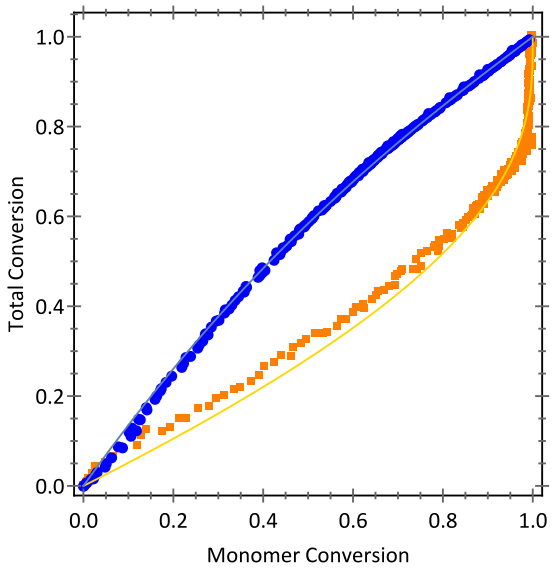

Total conversion versus monomer conversion data for the copolymerization of (□) allyl glycidyl ether and (●)ethylene oxide. (—) and (—) are model fits to the polymerization data using Equations 1 and 2.

4.3.2 Transport of CO_2 Reduction Products through Membranes

Measurement of multicomponent transport through membranes is rarely performed because it is difficult to accurately measure solute concentrations using conventional techniques (gas

chromatography, ion chromatography) that are not disruptive to the permeation of those solutes through the membrane. The permeability of membranes to CO_2 reduction reaction products was characterized using a novel method developed under this contract using *in situ* FTIR spectroscopy. This technique is capable of the simultaneous measurement of multiple component permeation, provided that each analyte has a distinct IR signature. Calibrations were prepared correlating IR intensity with analyte concentration for methanol, formate, and acetate using standard solutions of each over a concentration range of 0.01M – 1M. Although this concentration range is higher than the product concentraton that might be expected in a CO_2 reduction device, it is a useful range over which to characterize membrane transport characteristics. In this regime, diffusion coefficients of CO_2 reduction products are unlikely to be strongly concentration dependent. Therefore, membrane permeabilities determined in this concentration regime might reasonably be used to predict transport at lower concentrations. Extinction coefficients were calculated at several wavenumbers, as shown in Table 6.

Table 6: Extinction Coefficients of Methanol, Formate and Acetate

Wavenumber (cm^{-1})	Acetate	Methanol	Formate
1021.8	--	0.1285	--
1383.5	0.0859	--	0.1248
1413.4	0.2938	--	--

The experimental apparatus is shown in Figure 43. An FTIR probe is inserted in the receiver (left) chamber, which is initially filled with ultrapure water. The donor (right) chamber is initially filled with a 1M solution of the solute(s) of interest, and the concentration of the analyte(s) in the receiver chamber is measured as they diffuse from the donor chamber to the receiver chamber. Initial measurements were made using methanol, formate, and acetate on Nafion 117. While methanol transport through Nafion has been widely characterized, permeation data for other CO_2 reduction products are largely absent from literature.

Figure 44: *In situ* FTIR Measurement of CO_2 Reduction Product Permeation

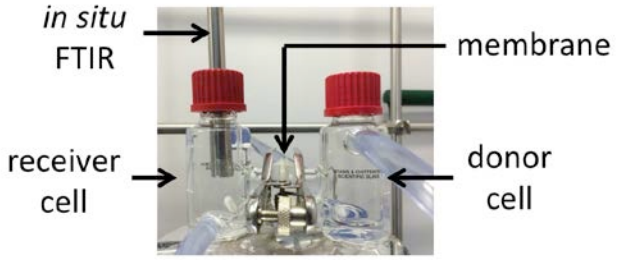

The permeabilities of Nafion 117 to methanol, acetate, and formate were determined using pure (1M) solutions and mixtures (1M equimolar) of these solutes. The increase in solute concentration of the receiver cell (initially filled with ultrapure water) was tracked as a function

of time. Time-resolved data were fit to the following expression to obtain permeabilities for solutes corresponding to the absorbance at a particular wavelength:

$$\ln\left(1 - 2\frac{M_t}{M_0}\right) = P_M\left(-\frac{2A}{Vl}t\right)$$

where M_t is the solute concentration in the receiver cell at time t, M_0 is the solute concentration in the donor cell (1M), P_M is the permeability, A is the membrane area, V is the half-cell volume (20 mL), and l is the membrane thickness. Permeabilities of methanol, formate, and acetate, measured as single solutes and in the presence of other solutes, are given in the Table 7. At least three replicates were performed for each value. The permeability of methanol matched literature values and was, therefore, used to establish the validity of the method. Values for the other permeabilities are not readily available in the literature.

Table 7: Measured Diffusive Permeabilities (cm^2/s) of CO_2 Reduction Products Through Nafion 117

Co-solute		Methanol	Formate	Acetate
	None	1.59E-06	8.03E-06	3.10E-06
	Methanol	--	1.71E-07	7.88E-08
	Formate	1.01E-06	--	9.28E-08
	Acetate	1.00E-06	1.69E-07	--

The permeability of Nafion 117 to all three solutes was measured using feed solutions of a single solute and of multiple solutes. The permeability of Nafion 117 to methanol was an order of magnitude higher than that of formate and two orders of magnitude higher than acetate. Nafion 117 contains sulfonate moieties, which are ionized and adopt a negative charge when the membrane is hydrated. Therefore, electrostatic repulsion between the negatively charged polymer matrix and the negatively charged formate and acetate ions contributes to a lower permeability of Nafion 117 to the charged solutes than the uncharged methanol. Acetate, as it is larger than formate, likely diffuses more slowly than formate through the polymer matrix, leading to its lower permeability than formate. These results could be validated using nuclear magnetic resonance spectroscopy to detect the evolution of methanol ^{13}C, formate ^{13}C, and acetate ^{13}C concentration in the receiver cell volume during future permeation studies.

4.3.3 Simulation of Diffusion within Polymer Electrolyte Membranes

The study of the molecular-level basis of transport within polymer electrolyte membranes (PEM's) is complicated by the length and time scales that must be simulated. The typical thickness of a PEM is 100 – 400 micrometers, which requires seconds for a solute to traverse. The Poisson-Boltzmann Semi-Analytical Method (PB-SAM) (Yap, E.H.; Head-Gordon, T. *J Chem Theor Comput* 6 (2010) 2214; 9 (2013) 2481) was investigated as a simulation method that can span the length and time scales relevant to transport within polymers yet also maintain molecular-level detail. PB-SAM maintains molecular-level detail through the use of polarizable, high-order (>10) multipole expansions of overlapping spheres.

As validation of the method, transporting a single explicit water molecule through a carbon nanotube (CNT) in implicit water was simulated. Results, shown in Table 8, are consistent with typical molecular dynamics (MD) simulations (Hughes et al. *J Phys Chem C* 116 (2012) 24943). The agreement between MD and PB-SAM, which is good, indicates PB-SAM is a promising method for simulation of transport within nanoscopic pores.

Table 8: Diffusion Constant (x10^{-9} m^2/s) of Water in Carbon Nanotubes

		Bulk	(10,10) CNT
MD	3D	2.63	1.16
	Z	2.57	2.39
PB-SAM	3D	2.30	0.85
	Z	2.30	2.30

Diffusion constants from MD and PB-SAM for 3-dimesional (3D) and 1-dimensional (Z) axial diffusion.

To investigate PEM, varying numbers of positively charged functional groups (tetra-methyl ammonium) were placed randomly throughout the polymer region; an example is shown in Figure 44. The mean first passage time (MFPT) are summarized in Table 9 for the solutes of interest.

Figure 45: Simulation of Diffusion Inside a Polymer

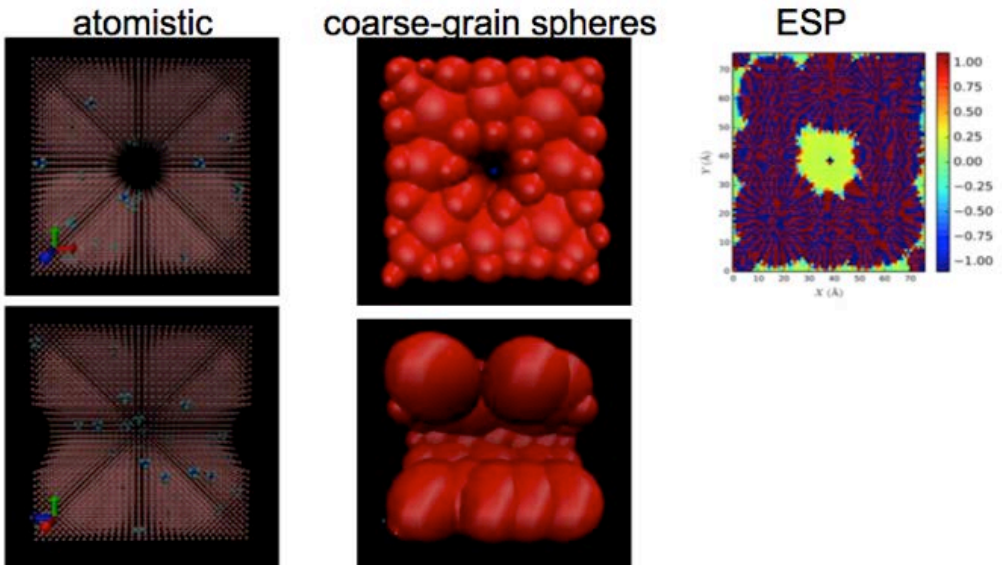

An atomistic representation is created with uncharged dummy atoms, from which a morphology is carved out. A random selection of dummy atoms are morphed into a functional group (tetramethyl ammonium). A Monte Carlo algorithm is used to grow coarse-grained spheres until the van der Waals surface is reproduced, and all atoms are enclosed within a sphere. The electrostatic potential can then be calculated using PB-SAM.

Table 9: Mean First Passage Time (MFPT) of CO_2 Reduction Products

Solutes		**Polymer**		
	q	NoES (Q = 0)	Q = +10	Q = +100
Methanol	0	5.0	4.8	3.1
Formate	-1	5.2	91	>900
Bicarbonate	-1		120	
Carbonate	-2		650	

Mean first passage time, measured in nanoseconds, as a function of solute charge (q) and polymer charge (Q). The polymers with "NoES" have their electrostatic forces turned off, such that the solutes move only under Brownian motion.

In summary, during the performance period researchers focused on discovery and preparation of membrane materials suitable for CO_2 reduction devices. They successfully narrowed down the scope of possible materials and useful synthetic methods, and identified a promising new platform. New techniques for controlling synthesis and measuring permeation of organic species through the membranes have also been developed.

CHAPTER 5:
Task 6: Technology Transfer Activities

5.1 Introduction

Since its inception, Joint Center for Artificial Photosynthesis (JCAP) has generated Intellectual Property (IP) relevant to artificial photosynthesis technologies, including inventions relating to the design of integrated solar-fuel generator prototypes, the discovery of new catalytic and light absorbing materials, and the development of new scientific methods and processes pertaining to solar-fuels research methods. In its R&D efforts sponsored by the California Energy Commission, JCAP produced additional IP disclosures.

An important objective of JCAP's IP Management Plan is to leverage the existing organizational expertise, capabilities, and resources of Caltech's and LBNL's institutional technology transfer offices. Specifically, the JCAP IP Management Plan is designed to provide JCAP's institutional technology transfer representatives and their designated IP attorneys with technological guidance and support during all key stages of IP development, including: (1) invention development and disclosure, (2) patent conversion planning, (3) prosecution and maintenance, and (4) commercial licensing. As detailed below, JCAP's management and research staff offer support to institutional representatives through a series of established processes to ensure the efficient advancement and commercialization of promising IP developed under the CEC contract.

All JCAP member institutions have affirmed their commitment to JCAP's IP management plan through adoption of the JCAP inter-institutional agreement (IIA). Specifically, the IIA provides for the coordination of invention disclosure, patent filing, and patent prosecution procedures, among JCAP partners institutions. Further, the IIA also provides terms for streamlined licensing of IP, including IP jointly owned by multiple JCAP partner institutions, to licensees for commercial development.

5.2 Invention Development and Disclosure

During the discovery and invention stage, JCAP supports the technology transfer process by routinely monitoring JCAP research outputs for possible patent filing opportunities and preparing and submitting patent disclosures for provisional patent filings.

Although researchers will be responsible for self-identifying promising developments as discoveries are made, JCAP management will also review all research manuscripts and presentations for potential IP prior to publication and encourage preparation and submission of invention disclosures when appropriate.

5.3 Support of Institutional Patent Conversion Activities

Following the submission of initial patent disclosures to institutional technology transfer offices, JCAP will continue to offer support, as needed, by providing (1) strategic guidance for

overall patent portfolio management activities, and (2) technological support for individual filings. To ensure the development of robust patent portfolios that protect JCAP's discoveries in an efficient manner, that are of commercial interest, and that most effectively utilize institutional patent budgets, JCAP's management works with institutional technology transfer representatives to help identify filings that are selected effectively for conversion to non-provisional status.

To assist with filing decisions, JCAP management can provide early assessments of commercialization and licensing potential and provide guidance for foreign filing opportunities. For provisional patents that are selected for conversion, individual JCAP researchers responsible for a specific invention can lend direct technical support to IP attorneys to draft the non-provisional patent filings.

5.4 Support of Institutional Prosecution and Maintenance Activities

Once non-provisional patents have been filed, JCAP will lend further support, as needed, for patent prosecution and maintenance activities. In addition to providing technical guidance to IP attorneys during this phase, JCAP will also assist the Caltech and LBNL institutional technology transfer offices with on-going assessments of commercialization potential based on input from both its industry partners and its own life-cycle and techno-economic analyses.

5.5 Support of Institutional Licensing Activities

Upon the initial submission of provisional invention disclosures, JCAP will support institutional efforts to identify prospective commercial licensees for JCAP IP. JCAP will research and identify any potential licensees at the outset of each discovery, and when appropriate, initiate licensing discussions in coordination with institutional technology transfer representatives. JCAP will leverage both its industry partnership group as well as its broad network of research collaborators to identify prospective licensees. During licensing negotiations, JCAP will also provide support, as needed, to its institutional technology transfer offices.

GLOSSARY

Term	Definition
AB	Assembly Bill
Ach	Change rate per hour
ACH50	Air Changes per Hour (ACH) at 50 Pa. Used as a measure of building airtightness
AFR	air/fuel ratio
AGA	American Gas Association
ANSI	American National Standards Institute
APT	Automatic performance testing
Appliance Flue	The passage(s) within an appliance through which combustion products pass from the combustion chamber of the appliance to the draft hood inlet opening on an appliance equipped with a draft hood or to the outlet of the appliance on an appliance not equipped with a draft hood.
ASHRAE	American Society of Heating, Refrigerating, and Air Conditioning Engineers
ASTM	American Society for Testing and Materials
Backdrafting	The reversal of the ordinary (upward) direction of air flow in a chimney or flue when vented combustion appliances are operating
BPI	Building Performance Institute
CAS	Combustion appliance safety
Category Vented Appliance	An appliance that operates with a *non-positive* vent static pressure and with a vent gas temperature that *avoids* excessive condensate production in the vent.
Category II Vented Appliance	An appliance that operates with a *non-positive* vent static pressure and with a vent gas temperature that *can cause* excessive condensate production in the vent.
Category IV Vented Appliance	An appliance that operates with a *positive* vent static pressure and with a vent gas temperature that *can cause* excessive condensate production in the vent.
CAZ	Combustion appliance zone
CBPCA	California Building Performance Contractors Association
CBSC	California Building Standards Commission
Term	**Definition**

Ag	Silver
$AgNO_3$	Silver nitrate
Au	Silver
BPG	Basal-plane graphite
Caltech	California Institute of Technology
CB[n]	Cucurbituril molecules; n denotes the number of the repeating units and can be 5,6,7, or 8
CEC	California Energy Commission
CEPS	Combinatorial Electro-Polymerization System
CFDS	Combinatorial Fuel Detection System
CH_4	Methane
CIT	California Institute of Technology
CNT	Carbon nanotube
CO	Carbon monoxide
Co	Cobalt
CoPc	Cobalt phthalocyanine
CO_2	Carbon dioxide
CO_2RR	Carbon dioxide reduction reaction
CPE	Controlled potential electrolysis
Cu	Copper
Cu-CfNT	Copper-covalently functionalized nanotubes
Cu-CNT	Copper-carbon nanotubes
Cucurbituril	Macrocyclic molecules
Cu-EDA-CNT	Carbon nanotubes containing grafted amines
C_2H_4	Ethylene
C_2H_6	Ethane
Enantiomer	One of two isomers that are mirror images of each other
EPG	Edge-plane graphite
EPR	Electron paramagnetic resonance to study compounds with unpaired

	electrons
Faradaic efficiency	The efficiency in which charge is transferred
Fe	Iron
FT-IR	Fourier-transform infrared
GC	Gas chromatography
Glass frit	Glass formed by the fusing and quenching ceramic composition
HER	Hydrogen evolution reaction
HPLC	High-pressure liquid chromatograph
HTE	High throughput experimentation
HTS	High Throughput Screening
H_2	Hydrogen
H_2SO_4	Sulfuric acid
IIA	Inter-institutional agreement
IP	Intellectual Property
IR	Infrared
JCAP	Joint Center for Artificial Photosynthesis
LBNL	Lawrence Berkeley National Laboratory
LGC	Liquid gas chromatography
Ligand	An ion or molecule that bonds to a metal ion to form a coordination complex
LPG	Liquefied petroleum gas
mA cm^{-1}	Milliampere per centimeter
MD	Molecular dynamics
MFPT	Mean first passage time
MIMS	Membrane inlet mass spectrometer
Mn	Manganese
MolCat	Molecular Catalysts
MSDS	Material safety data sheet

Ni	Nickel
$Ni(CO)_4$	Nickel carbonyl
NMR	Nuclear magnetic resonance
N_2	Nitrogen
PB-SAM	Poisson-Boltzmann Semi-Analytical Method
PEM	Polymer Electrolyte Membranes
Potentiostat	Instrument that measures the potential difference between an electrode and a reference electrode
PPE	Personal protective equipment
PPGE	Polyphenyl glycidyl ether
ppm	Parts per million
PPO	Poly(2,6-dimethyl phenylene oxide)
P2VP	Poly-2-vinylpyridine
P4VP	Poly-4-vinylpyridine
Racemic	Equal amounts of both enantiomers of a compound
RDE	Rotating disk electrode
RDEVs	Rotating disk electrode voltammograms
Resin	A solid or highly viscous polymer
RHE	Reversible hydrogen electrode
RID	Refractive index detector
ROP	Ring-opening polymerization
RRDE	Rotating ring-disk electrode
SCE	Saturated calomel electrode
Supernatant	The liquid layer that lies above a solid layer as a result of centrifugation, settling, or precipitation
UV-Vis	Ultraviolet-Visible
XPS	X-ray photoelectron spectroscopy
^{13}C	Carbon-13

REFERENCES

1. C. W. Machan, C. J. Stanton III, J. E. Vandezande, G. F. Majetich, H. F. Schaefer III, C. P. Kubiak and J. Agarwal, *Inorg. Chem.*, 2015, DOI: 10.1021/acs.inorgchem.5b01715.
2. D. C. Lacy, C. C. L. McCrory and J. C. Peters, *Inorg. Chem.*, 2014, **53**, 4980-4988.
3. Hod, M. D. Sampson, P. Deria, C. P. Kubiak, O. K. Farha and J. T. Hupp, *ACS Catal.*, 2015, 6302–6309.
4. N. Elgrishi, M. B. Chambers and M. Fontecave, *Chem. Sci.*, 2015, **6**, 2522–2531.
5. J. D. Blakemore, A. Gupta, J. J. Warren, B. S. Brunschwig and H. B. Gray, *J. Am. Chem. Soc.*, 2013, **135**, 18288–18291.
6. M. D. Sampson, J. D. Froehlich, J. M. Smieja, E. E. Benson, I. D. Sharp and C. P. Kubiak, *Energy Environ. Sci.*, 2013, **6**, 3748–3755.
7. C. Costentin, S. Drouet, G. Passard, M. Robert and J.-M. Savéant, *J Am Chem Soc*, 2013, **135**, 9023–9031.
8. J. L. Inglis, B. J. MacLean, M. T. Pryce and J. G. Vos, 2012, **256**, 2571–2600.
9. M. Bourrez, F. Molton, S. Chardon-Noblat and A. Deronzier, *Angew. Chem. Int. Ed.*, 2011, **50**, 9903–9906.
10. E. E. Benson, C. P. Kubiak, A. J. Sathrum and J. M. Smieja, *Chem. Soc. Rev.*, 2008, **38**, 89.
11. M. Isaacs, J. C. Canales, M. J. Aguirre, G. Estiu, F. Caruso, G. Ferraudi and J. Costamagna, *Inorg. Chim. Acta*, 2002, **339**, 224–232.
12. W. Leitner, *Angew. Chem. Int. Ed.*, 1995, **34**, 2207–2221.
13. J. P. Collin, J . P. Sauvage, *Coord. Chem. Rev.*, 1989, **93**, 245–268.
14. T. R. O'Toole, B. P. Sullivan, M. R. M. Bruce, L. D. Margerum, R. W. Murray and T. J. Meyer, *J. Electroanal. Chem.*, 1989, **259**, 217–239.
15. M. Hammouche, D. Lexa, J. M. Savéant and M. Momenteau, *J. Electroanal. Chem.*, 1988, **249**, 347–351.
16. M. Beley, J.P. Collin, R. Ruppert and J.P. Sauvage, *J. Am. Chem. Soc.*, 1986, **108**, 7461–7467.
17. C. R. Cabrera and H. D. Abruña, *J. Electroanal. Chem.*, 1986, **209**, 101–107.
18. M. Isaacs, F. Armijo, G. Ramírez, E. Trollund, S. R. Biaggio, J. Costamagna and M. J. Aguirre, *J. Mol. Cat. A: Chem.*, 2005, **229**, 249–257.
19. T. Abe, H. Imaya, T. Yoshida, S. Tokita, D. Schlettwein, D. Wöhrle and M. Kaneko, *J. Porphyrins Phthalocyanines*, 1997, **01**, 315–321.
20. H. Aga, A. Aramata and Y. Hisaeda, *J. Electroanal. Chem.*, 1997, **437**, 111–118.
21. J. H. Zagal, *Coord. Chem. Rev.*, 1992, **119**, 89–136.
22. T. Atoguchi, A. Aramata, A. Kazusaka and M. Enyo, *J. Electroanal. Chem.*, 1991, **318**, 309–320.
23. K. Kusuda, R. Ishihara, H. Yamaguchi and I. Izumi, *Electrochim. Acta*, 1986, **31**, 657–663.
24. S. Kapusta and N. Hackerman, *J. Electrochem. Soc.*, 1984, **131**, 1511–1514.

25. C. M. Lieber and N. S. Lewis, *J. Am. Chem. Soc.*, 1984, **106**, 5033–5034.

26. S. Meshitsuka, M. Ichikawa and K. Tamaru, *J. Chem. Soc., Chem. Commun.*, 1974, 158–159.

27. T. Abe, T. Yoshida, S. Tokita, F. Taguchi, H. Imaya and M. Kaneko, *J. Electroanal. Chem.*, 1996, **412**, 125–132.

28. T. Yoshida, K. Kamato, M. Tsukamoto, T. Iida, D. Schlettwein, D. Wöhrle and M. Kaneko, *J. Electroanal. Chem.*, 1995, **385**, 209–225.

29. S. Lin, C. S. Diercks, Y.-B. Zhang, N. Kornienko, E. M. Nichols, Y. Zhao, A. R. Paris, D. Kim, P. Yang, O. M. Yaghi and C. J. Chang, *Science*, 2015, **349**, 1208–1213.

30. J. J. Walsh, C. L. Smith, G. Neri, G. F. S. Whitehead, C. M. Robertson and A. J. Cowan, *Faraday Discuss.*, 2015.

31. D. Saravanakumar, J. Song, N. Jung, H. Jirimali and W. Shin, *ChemSusChem*, 2012, **5**, 634–636.

32. J. A. Ramos Sende, C. R. Arana, L. Hernandez, K. T. Potts, M. Keshevarz-K and H. D. Abruña, *Inor. Chem.*, 1995, **34**, 3339–3348.

33. T. Yoshida, K. Tsutsumida, S. Teratani, K. Yasufuku and M. Kaneko, *J. Chem. Soc., Chem. Commun.*, 1993, 631–633.

34. S. Aoi, K. Mase, K. Ohkubo and S. Fukuzumi, *Chem. Commun.*, 2015, **51**, 10226–10228.

35. P. Kang, T. J. Meyer and M. Brookhart, *Chem. Sci.*, 2013, **4**, 3497–3502.

36. J. Schneider, H. Jia, K. Kobiro, D. E. Cabelli, J. T. Muckerman and E. Fujita, *Energy Environ. Sci.*, 2012, **5**, 9502–9510.

    A. Koca, M. Kasimsener, M. Kocak and A. Gul, *Int. J. of Hydrogen Energy*, 2006, **31**, 2211–2216.

37. O. Osmanbas, A. Koca, M. Kandaz and F. Karaca, *Int. J. of Hydrogen Energy,* 2008, **33**, 3281–3288.

    A. Koca, A. Kalkan and Z. A. Bayır, *Electrochim. Acta*, 2011, **56**, 5513–5525.

38. F. Zhao, J. Zhang, T. Abe, D. Wöhrle and M. Kaneko, *J.l of Mol. Cat. A: Chem.*, 1999, **145**, 245–256.

39. T. Nyokong, *Polyhedron*, 1995, **14**, 2325–2329.

40. R. J. Lim, M. Xie, M. A. Sk, J.-M. Lee, A. Fisher, X. Wang and K. H. Lim, *Catal. Today*, 2013, **233**, 169–180.

41. K. J. P. Schouten, E. Pérez Gallent and M. T. M. Koper, *ACS Catal.*, 2013, **3**, 1292–1295.

42. K. P. Kuhl, E. R. Cave, D. N. Abram and T. F. Jaramillo, *Energy Environ. Sci.*, 2012, **5**, 7050–7059.

43. M. Gattrell, N. Gupta and A. Co, *J. Electroanal. Chem.*, 2006, **594**, 1–19.

44. K. P. Kuhl, T. Hatsukade, E. R. Cave, D. N. Abram, J. Kibsgaard and T. F. Jaramillo, *J. Am. Chem. Soc.*, 2014, **136**, 14107–14113.

45. Y. Hori, A. Murata and R. Takahashi, *J. Chem. Soc., Faraday Trans. 1*, 1989, **85**, 2309–2326.

46. Y. Hori, A. Murata, K. Kikuchi and S. Suzuki, *J. Chem. Soc., Chem. Commun.*, 1987, 728–

729.

47. Y. Chen, C. W. Li and M. W. Kanan, *J. Am. Chem. Soc.*, 2012, **134**, 19969–19972.
48. G. J. Samuels and T. J. Meyer, *J. Am. Chem. Soc.*, 1981, **103**, 307–312.
49. J. M. Calvert and T. J. Meyer, 1982, **21**, 3978–3989.
50. C. Riplinger, M. D. Sampson, A. M. Ritzmann, C. P. Kubiak and E. A. Carter, *J. Am. Chem. Soc.*, 2014, **136**, 16285–16298.
51. 1. G. Ung, J. Rittle, M. Soleilhavoup, G. Bertrand, J. C. Peters, *Angew. Chem. Int. Ed.* **2014**, *53*, 8427.
52. 2. V. Lavallo, Y. Canac, C. Prasang, B. Donnadieu, G. Bertrand, *Angew. Chem. Int. Ed.* **2005**, *44*, 5705.
53. 3. G. Ung, J. C. Peters, *Angew. Chem. Int. Ed.* **2015**, *54*, 532.
54. 1. Yanwei Lum, Youngkook Kwon, Peter Lobaccaro, Le Chen, Ezra. L. Clark, Alexis T. Bell, Joel W. Ager. Trace Levels of Copper in Carbon Materials Show Significant Electrochemical CO_2 Reduction Activity, ACS Catalysis, 6, 202-209, (2016).
55. 1. Yanwei Lum, Youngkook Kwon, Peter Lobaccaro, Le Chen, Ezra. L. Clark, Alexis T. Bell, Joel W. Ager. Trace Levels of Copper in Carbon Materials Show Significant Electrochemical CO_2 Reduction Activity, ACS Catalysis, 6, 202-209, (2016).
56. Beckingham, B.S.; Sanoja, G.E.; Lynd, N.A. “Simple and Accurate Determination of Reactivity Ratio Using a Nonterminal Model of Chain Copolymerization” Macromolecules, 2015, 48 (19), 6922-6930.